USAAVLABS TECHNICAL REPORT 67-37

PERFORMANCE AND STRESSES OBTAINED ON AN ISOLATED VTOL-TYPE PROPELLER OPERATING IN HOVERING, TRANSITIONAL, AND AXIAL FLIGHT

By

Andrew R. Trenka

August 1967

U. S. ARMY AVIATION MATERIEL LABORATORIES
FORT EUSTIS, VIRGINIA

CONTRACT DA 44-177-AMC-75(T)

CORNELL AERONAUTICAL LABORATORY, INC.

BUFFALO, NEW YORK

97

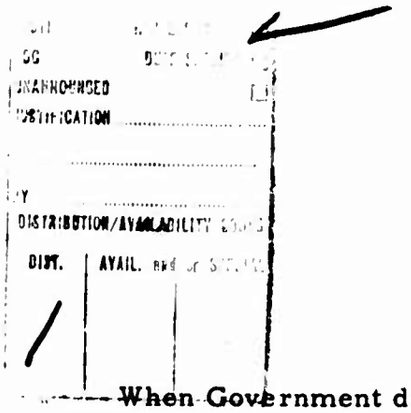

Disclaimers

When Government drawings, specifications, or other data are used for any purpose other than in connection with a definitely related Government procurement operation, the United States Government thereby incurs no responsibility nor any obligation whatsoever; and the fact that the Government may have formulated, furnished, or in any way supplied the said drawings, specifications, or other data is not to be regarded by implication or otherwise as in any manner licensing the holder or any other person or corporation, or conveying any rights or permission, to manufacture, use, or sell any patented invention that may in any way be related thereto.

Disposition Instructions

Destroy this report when no longer needed. Do not return it to originator.

DEPARTMENT OF THE ARMY
U. S. ARMY AVIATION MATERIEL LABORATORIES
FORT EUSTIS, VIRGINIA 23604

This report has been reviewed by the U. S. Army Aviation Materiel Laboratories and is considered to be technically sound. The report is published for the exchange of information and the stimulation of ideas.

Task 1F125901A142
Contract DA 44-177-AMC-75(T)
USAAVLABS Technical Report 67-37
August 1967

PERFORMANCE AND STRESSES OBTAINED ON AN ISOLATED VTOL-TYPE PROPELLER OPERATING IN HOVERING, TRANSITIONAL, AND AXIAL FLIGHT

CAL Report BB-1846-S-2

By

Andrew R. Trenka

Prepared by
Cornell Aeronautical Laboratory, Inc.
Buffalo, New York

for

U. S. ARMY AVIATION MATERIEL LABORATORIES
FORT EUSTIS, VIRGINIA

SUMMARY

Experimental performance and blade stresses measured on a three-bladed VTOL-type propeller tested in free air are presented. The isolated propeller was tested over ranges of prop speed, forward velocity, blade angle setting, and thrust axis to free-stream angle.

Correlation with a theoretical method of predicting propeller performance and blade stresses was made. It was found that when the propeller was operating in a flight condition for which the theory was developed, correlation between theory and experiment was good. When the propeller was operating in a flight condition where very small positive or negative effective angles of attack were encountered, correlation between theory and experiment was poor.

FOREWORD

The technical effort reported herein was conducted at Cornell Aeronautical Laboratory, Inc., during the period from June 1965 to January 1967. Mr. Andrew R. Trenka was the project engineer. This program was sponsored by the U. S. Army Aviation Materiel Laboratories, Fort Eustis, Virginia, and was administered by Mr. John E. Yeates.

Recognition is given to Dr. I. C. Statler and Mr. R. P. White, Jr., for their assistance.

CONTENTS

ILLUSTRATIONS

LIST OF TABLES

LIST OF SYMBOLS

C_P	power coefficient = $2\pi Q/\rho n^2 D^5$
C_T	thrust coefficient = $T/\rho n^2 D^4$
D	propeller diameter, ft
J	advance ratio = V_f/nD
J'	modified advance ratio = $V_f \cos\tau/nD$
NF	propeller normal force, lb
$\overline{NF}$	component of inplane force measured by the rotating balance, lb
n	propeller speed, cps
PM	propeller pitching moment, ft-lb
$\overline{PM}$	component of inplane moment measured by the rotating balance, ft-lb
Q	propeller torque, ft-lb
SF	propeller side force, lb
T	propeller thrust, lb
V_f	free-stream velocity, ft/sec
YM	propeller yawing moment, ft-lb
α_e	effective angle of attack, deg
α_I	induced angle of attack, deg
β	local geometric blade angle, deg
β_R	reference geometric blade angle, deg
η	efficiency = $(C_T/C_P)J$
θ	angle of attack due to torsional deformation, deg
ρ	air density, slug/ft^3

τ	angle free-stream velocity makes with thrust axis, deg
ψ	azimuthal position of blade, deg
Ω	propeller speed, rpm
ω_{wu}	frequency of wind-speed indicators, cps

INTRODUCTION

Recent efforts to develop V/STOL aircraft prototypes have demonstrated that existing means for predicting propeller performance in the static and transitional flight modes are inadequate. Attempts to alleviate this situation are being made under U. S. Army sponsorship at Cornell Aeronautical Laboratory, Inc., (CAL) (Reference 1) and at other research establishments (Reference 2). These recent advances characteristically involve the use of high-speed digital computing machines to carry out the necessary calculations.

The method for predicting propeller performances and blade stresses developed at CAL (Reference 1) can treat the static, transitional, and axial flight cases. Included in this mathematical model are the effects of wake contraction (for the hovering case), consideration of finite number of blades, provisions for incorporation of experimental sectional airfoil characteristics, effects of structural deformations, and first-order effects of wing and nacelle interferences on the blade aerodynamic loading.

During a previous program, an attempt was made to correlate the CAL theory with data collected at NASA Ames in the 40-foot by 80-foot low-speed wind tunnel. Data which were obtained on a 0.6 scale model of the XC-142 are presented in Figure 18 of Reference 1. The experimental error associated with the measurement of the thrust and torque during those tests was estimated to be $\pm$10 percent. The theoretically predicted values of thrust generally fell within this $\pm$10-percent error band. The theoretically predicted values of torque were generally slightly higher than the 10-percent error band.

Since the experimental data were not considered to be sufficiently accurate and, furthermore, included interference effects (propeller-propeller overlap, fuselage and wing-tip end effects) not included in the present mathematical model, no definitive evaluation of the theoretical method was made. Instead, it was recommended that accurate performance data be collected on an isolated propeller operating in hovering, transitional, and axial flight for the purpose of correlation with the newly developed theory and any subsequent theories.

As an outgrowth of that recommendation, the effort reported herein was undertaken. The purpose of these tests was to obtain thrust, torque, and inplane forces and moments on an isolated propeller operating in hovering, transitional, and axial flight. Blade strain data were also to be obtained. The parameters which were varied were free-stream velocity (V_f), propeller speed (Ω), blade angle (β_R), and angle which the thrust axis makes with the free-stream velocity (τ). Correlation with theoretically predicted propeller performance and blade stresses was to be performed.

DESCRIPTION OF THE TEST APPARATUS

SMALL ROTOR TEST FACILITY

The tests were conducted on a test bed developed by CAL for the U. S. Army in 1959. The facility, shown in Figure 1, consists of a modified tractor-trailer combination capable of speeds up to 60 miles per hour. The tractor is basically a standard truck chassis whose body was modified to be aerodynamically streamlined. At the rear of the tractor is a rearward-facing seat for the test observer and the remote controls for the test conditions and data recording on the trailer. The trailer consists of a large flat bed from which protrudes a tower whose height is adjustable in fixed increments. Slung beneath the trailer bed are: two motor-generator sets which supply up to 5,000 watts of power; a 375-horsepower automotive engine which supplies power to drive a test model via a right-angle gear drive and power shafting attached to the tower; water and gasoline supplies for the engine; a radiator and an oil pump for cooling of the right-angle gear drive; control panels for operating various components of the facilities; and data recording equipment. Mounted at the top of the tower is a pully box which transfers power from the main drive shaft coming up from the engine to a second shaft whose centerline is coincident with the centerline of the tower. The entire trailer assembly is mounted on an air suspension system designed to cushion the trailer from road roughness and to maintain the trailer bed horizontal at all times. For a more detailed description of the basic facility, see Reference 3.

MODIFICATIONS TO THE SMALL ROTOR TEST FACILITY

In order to allow testing of an isolated propeller on the above facility, a large pod was designed and fabricated (see Figure 2). The pod, which is mounted atop the tower, houses a right-angle gear drive (similar to the one slung beneath the trailer bed) which transfers rotational

power from the vertical shaft of the pully box to a horizontal shaft. This shaft is supported by two angular contact bearings and itself supports a slip-ring assembly, force balance unit, and the propeller. The pod has a counterbalance attached to its rear face to insure that the center of gravity of the entire unit is located on the centerline of the tower. The pod assembly is mounted on a turntable which allows rotation in a horizontal plane through 360 degrees in 5-degree increments.

A radiator and an oil pump for cooling the upper right-angle drive were also added.

The slip-ring assembly mounted on the shaft in the pod has 44 rings. The unit is supported on 2 ball-bearing rings, one at each end. The silver graphite, chemopolarized brushes are mounted on readily removable brush blocks and ride on coin-silver rings.

The propeller set which was tested consisted of three right-handed blades. These blades are similar to the ones employed on the 0.6 scale model of the XC-142. The blade planform characteristics are presented in Figure 3. The blades were mounted in a standard hub assembly with a pitch-change mechanism powered by a 28-volt dc supply. Although the capability for changing blade pitch angle remotely could have been incorporated, it was felt that it was not worth the additional effort required. Thus, provisions were made which permitted a blade-angle change only when the prop was stationary.

MEASURING DEVICES

Rotating Balance

To measure the instantaneous values of the shaft loads, a four-component balance system designed and built by NASA was employed. This unit was mounted on the end of the power shaft, and the

prop was then hung from the opposite end of the balance. The balance rotated with the prop and shaft. Thus, all loads from the prop were transferred to the shaft via the balance.

The balance measures thrust and torque directly. However, the character of the balance is such that it measures only a component of the inplane force and moment (i.e., the force and moment acting in the plane of the prop). In order to determine the magnitudes and directions of the total inplane force and moment from the balance outputs, these loads must be periodic. Further discussion of the balance is presented in subsequent sections and in Appendix I.

Strain Rosettes

The instantaneous strain on the camber side of the blade was measured at four spanwise stations (see Figure 4). At each station, a 45-degree strain rosette (three strain gages mounted at 45-degree angles with respect to one another) was bonded to the blade surface. The gages were SR-4, type FABR-50-35/S-13. The resistance of each gage in the rosette was 350 $\pm$ 2.5 ohms and each had a gage factor of 2.13 $\pm$ 1 percent. Each gage of each strain rosette was wired into one arm of a Wheatstone bridge. The remaining three arms of the bridge were made up of 0.5 watts, 350 ohms $\pm$ 0.1-percent resistors.

Miscellaneous

To measure wind speed and direction, two wind-speed indicators and one wind-direction indicator were mounted at the front of the trailer deck. One of the speed indicators was connected to a tachometer in the tractor and was used by the driver to set the desired test forward velocity. The second wind-speed indicator signal and the wind-direction indicator signal were recorded during each test run on the oscillograph records for data reduction purposes.

The minimum blade pitch angle was determined by the low-pitch stop (a mechanical limit) which was an integral part of the hub assembly. There was a similar high-pitch stop. Both were adjustable within limits. The low-pitch stop was set at its minimum value which for the blades tested was 5 degrees at the 64.4-percent span. The high-pitch stop was set at 20 degrees at the 64.4-percent span. The intervening span was divided into 1-degree increments from 5 degrees to 20 degrees. Thus, by carefully lining up a pointed indicator mounted on the hub with scribe marks on the blade shank, the blade angle at the 64.4-percent span could be determined to within about $\pm$0.5 degree.

The prop speed was measured using an electromagnetic device mounted in the pod assembly. The completion of a magnetic circuit between a pin and a plunger once per revolution generated an electrical pulse which was recorded.

RECORDING EQUIPMENT

All recording equipment was mounted on the test facility (see Figure 1).

Recording was performed on a 3-kilocycle carrier system consisting of 16 amplifiers, 2 oscillographs, and 2 magazines. Each balance and strain-gage signal was fed into an amplifier and then into the oscillograph. Signals recorded directly on the oscillograph were: prop speed, wind velocity and direction, a 100-cps timing trace, and a synchronizing trace which allowed correlation in time between the two oscillographs.

The recording equipment could be activated remotely from the observer's post in the tractor.

In addition to the above recording, certain of the data signals were displayed on a panel in the observer's post for the purpose of control and as a safety check. Figure 5 shows this panel. Displayed are

engine and prop speeds for the purpose of control. For the purpose of safety, the upper and lower gearbox oil temperature as well as prop thrust and torque were monitored — the latter so that maximum safe prop loads would never be exceeded, and the former to warn of dangerously high temperatures in the right-angle gear drives.

Also located in the observer's post was the control which governed propeller speed.

CALIBRATION OF THE MEASURING DEVICES

CALIBRATION OF THE ROTATING BALANCE

Pretest Calibration

Special attention was given to the unusual characteristics of the rotating balance. For example, care was taken so that the inplane force and moment calibrations were made along the most sensitive balance axes. The calibration matrix obtained from static calibration of the balance is presented in Table I. The coefficients are given in terms of load per meter unit. Thrust and $\overline{NF}$ coefficients are in pounds per meter unit, and torque and $\overline{PM}$ are in foot-pounds per meter unit. The meter unit is defined as the deflection which would be obtained on a measuring device (meter) when a prespecified resistance is placed in parallel across a prespecified arm of one of the balance bridges. The numbers in parentheses in Table I are those values obtained when the balance was loaded negatively. ($\overline{NF}$ and $\overline{PM}$ are the measured components of the total inplane force and moment.) For a definition of positive loads, see Figure 6.

TABLE I
ROTATING BALANCE CALIBRATION MATRIX

	THRUST	TORQUE	$\overline{NF}$	$\overline{PM}$
THRUST	1.686536 (1.6868710)	0.031305 (-0.000199)	-0.02627 (-0.015816)	0.001836 (-0.031632)
TORQUE	0.0000270 (-0.000290)	0.85573 (0.857619)	-0.015686 (-0.007320)	0.001435 (0.004193)
$\overline{NF}$	-0.0008430 (-0.0008370)	0.012272 (0.013874)	0.589132 (0.592773)	-0.060163 (-0.0615910)
$\overline{PM}$	-0.0082910 (-0.008208)	0.028247 (0.029394)	-0.255183 (-0.249581)	0.809439 (0.800671)

The value of the resistance required to produce 1,000 meter units of deflection in each performance channel is presented in Table II.

Table II
RESISTANCE REQUIRED TO PROVIDE 1,000 METER UNITS OF DEFLECTION

CHANNEL	RESISTANCE
THRUST	1.60×10^5 ohms
TORQUE	0.84×10^5 ohms
$\overline{NF}$	1.22×10^5 ohms
$\overline{PM}$	2.32×10^5 ohms

When the above resistances were placed across their respective bridge arms and recorded on the oscillograph equipment described previously, the resultant trace deflections obtained were (for the noted attenuator settings on their amplifiers) those indicated in Table III.

Table III
OSCILLOGRAPH TRACE DEFLECTIONS FOR PRESCRIBED RESISTANCE

CHANNEL	ATTENUATION SETTING	OSCILLOGRAPH TRACE DEFLECTION
THRUST	100	2.40 inches
TORQUE	200	2.18 inches
$\overline{NF}$	150	2.14 inches
$\overline{PM}$	100	1.78 inches

The attenuator setting represents the relative increase or decrease of the output signal accomplished by the amplifier for a given input signal. This could be set at prespecified settings from 1 to 1,000. The largest increase in output signal was obtained at a setting of "1".

Thus, to compute the calibration matrix elements in terms of load per inch of oscillograph deflection, consider, for example, the thrust due to thrust element. To convert 1.686536 pounds of thrust per meter unit into pounds of thrust per inch of oscillograph deflection at any given attenuation, proceed as follows:

$$a_{TT} = (\bar{a}_{TT})(R_{TT})(O_{TT})(G_{TT}) \qquad (1)$$

where

a_{TT} = main thrust element in pounds of thrust per inch of oscillograph deflection

$\bar{a}_{TT}$ = main thrust element in pounds of thrust per meter unit — 1.686536 pounds per meter unit

R_{TT} = number of meter units caused by a prespecified resistance in parallel with a prespecified arm of the balance bridge — $\frac{1{,}000 \text{ meter units}}{1.6 \times 10^5 \text{ ohms}}$

O_{TT} = ratio of prescribed resistance to resultant oscillograph trace deflection at a given amplifier attenuation — 1.6×10^5 ohms/2.4 inches

G_{TT} = ratio of new attenuation setting to attenuation setting when determining O_{TT} — new attenuation/100

Posttest Calibration

After the data had been collected, it was decided to perform a calibration of the balance while it was mounted on the test facility. The purpose was simply to obtain a check of the main diagonal elements of the matrix of Table II. The calibration of the torque, $\overline{NF}$, and $\overline{PM}$ components was done only statically, while the thrust was calibrated both statically and with the propeller shaft rotating at approximately 1200 rpm.

The static calibration of torque, $\overline{NF}$, and $\overline{PM}$ yielded the same main diagonal coefficients as obtained in the pretest calibration to within 5 percent on $\overline{NF}$ and $\overline{PM}$ and 2 percent on torque.

The static and dynamic calibrations of thrust indicated that a large hysteresis loop exists in the thrust load versus balance output curve. A nondimensionalized form of his curve is presented in Figure 7. The slope obtained while loading the balance is approximately 10 percent higher than the slope obtained upon unloading the balance. This hysteresis-loop measurement was repeated several times with the balance stationary as well as rotating. The mean of the slopes obtained in these posttest calculations agreed to within 2 percent with the slopes obtained in the pretest static calibration where the data reduction techniques had masked the hysteresis loop.

During the dynamic calibration, certain other anomalous behavior of the balance was noted. Specifically, it was noted that

(i) When a constant inplane force and moment existed, the response in the thrust component output of the balance due to these inplane loads varied nonlinearly with the azimuthal orientation of the load relative to the blades.

(ii) A similar, but smaller, effect was observed in the indicated torque response to inplane forces and moments.

(iii) The response in the $\overline{NF}$ component output of this balance, due to a constant applied inplane moment, also varied nonlinearly with azimuth as did the response in the $\overline{PM}$ component due to a constant inplane force.

To substantiate these observations, a calibration of the thrust component was devised in which a fixed normal force load of 581 pounds was hung in the plane of the propeller. With the balance in a known angular position, specified as zero, a pure thrust load of known magnitude was applied. A record of all balance components was made. Without changing any of the loads, the balance was indexed by hand through prespecified angular positions and records were taken at each position. The balance was returned to the zero angular position, the next thrust load increment was added, and the procedure was repeated. The slope of the thrust load versus the thrust deflection was a constant for all azimuthal positions and agreed with the results previously obtained to within ± 2 percent. However, the variation of the thrust response due to the inplane load was a nonlinear function of azimuthal orientation of the balance. This is shown in Figure 8 where plots of T, $\overline{NF}$, and $\overline{PM}$ responses in the form of nondimensionalized oscillograph deflection versus azimuthal orientation of the balance are presented. Data were recorded every 20 degrees of azimuth for each applied thrust load. The deflection in each balance component at $\psi = 0$ for each thrust load was subtracted from the respective deflections at each of the other azimuthal positions. This effectively removed the deflections due to the thrust load. The trace deflections which remained were due to coupling from the constant inplane force and moment. Further, since the inplane force and moments were constant, the coupling-induced deflections all collapsed to the single curves shown in Figure 8 for all thrust loadings. The variation in torque due to the inplane load was negligibly small. Note that all of the responses are sinusoidal. However, the $\overline{PM}$ component is approximately 180 degrees out of phase

with the $\overline{NF}$ component, and the T component is approximately 130 degrees out of phase with $\overline{NF}$.

From the above calibrations and several other selective tests, it was concluded that

(i) The main diagonal terms of thrust and torque in the calibration matrix were independent of the magnitude of the applied load and of the azimuthal orientation of the balance.

(ii) For any given azimuthal position of the balance, the slope of the applied inplane load versus balance output for that channel was independent of the load. Further, the angular position of maximum balance sensitivity to inplane loads was known, and the corresponding calibration constants were those employed in the calibration matrix of Table I.

(iii) The effects of inplane loads on the outputs of the thrust, $\overline{NF}$, and $\overline{PM}$ components of the balance were nonlinear functions of the azimuthal position of the balance. The nonlinear coupling effect was more pronounced between $\overline{NF}$ and $\overline{PM}$ than between either $\overline{NF}$ and T or $\overline{PM}$ and T.

To define the magnitudes of the nonlinear coupling terms accurately would have required considerable additional effort. It was decided that this effort was unwarranted at this time in view of the ± 5 percent uncertainty in the thrust calibration constant due to the hysteresis loop and the belief that, even if the coupling terms listed in Table I were in error by 100 percent, their effect upon the evaluation of the mean thrust load would be small. Hence, the matrix of Table I was employed to reduce the experimental data.

While the mean loads will probably not be much affected by the errors due to the uncertain magnitude and character of the coupling terms, the fundamental and higher harmonics will be seriously affected.

CALIBRATION OF THE STRAIN GAGES

A test beam consisting of a cantilevered aluminum bar 6.25 inches by 1.75 inches by 0.0625 inch was instrumented with a strain rosette of the same type mounted on the prop. The test rosette was wired into a bridge network similar to the ones employed on the prop. The output from the bridge was connected to an open set of slip rings to allow recording of the signal on the equipment mounted on the test facility. The beam was then loaded, incrementally, with a tip-applied load, and records were taken at each loading. The test was repeated with the bridge output connected to a strain analyzer. The strain of each gage at each applied load was read and recorded.

Plots of applied load versus oscillograph deflection and strain were made. From these plots, a plot of strain versus oscillograph deflection was obtained. From this plot was obtained the strain gage calibration constant. To account for anticipated differences in the electrical characteristics of the rosette systems mounted on the blade, a resistance was computed, which when placed in parallel with the bridge arm containing a strain gage, resulted in a 1-inch oscillograph trace deflection. The shunt resistance was then placed across each gage of the test beam and the blade. The test beam rosette output yielded a 1-inch trace deflection for each of its gages with an error of approximately ± 0.5 percent. The trace deflection obtained from each prop strain gage thus gave a measure of the resistance differences in each circuit due to line, slip rings, and amplifiers and could be used to modify the calibration constant obtained from the test beam strain rosette. With the amplifier attenuations for all strain gages set at "7", the resultant calibration constants are those presented in Table IV.

Table IV
STRAIN-GAGE CALIBRATION CONSTANTS

STATION	CALIBRATION CONSTANT INCHES/INCH OF TRACE DEFLECTION
1 - GAGE 1	31.2485×10^{-6}
GAGE 2	29.9065×10^{-6}
GAGE 3	30.6589×10^{-6}
2 - GAGE 1	30.0911×10^{-6}
GAGE 2	31.3154×10^{-6}
GAGE 3	26.9324×10^{-6}
3 - GAGE 1	25.3016×10^{-6}
GAGE 2	30.3724×10^{-6}
GAGE 3	62.3638×10^{-6}
4 - GAGE 1	29.3366×10^{-6}
GAGE 2	28.5352×10^{-6}
GAGE 3	32.0006×10^{-6}

CALIBRATION OF THE BLADE PITCH ANGLE

The hub with the blades mounted was placed on a level reference plate. A reference mark was made on each blade at the 64.4-percent span. Using an inclinometer, the blade angle at the low-pitch stop position was measured. It was found to be 5.200 degrees, 5.317 degrees, and 5.167 degrees for the three blades measured. At the high-pitch stop position, the blade angles measured were 20.083 degrees, 19.700 degrees, and 20.384 degrees. To determine how well intermediate blade angles could be set, the blade was set using the pitch-change mechanism at 10 degrees and 15 degrees many times. It was found that the intermediate angles could be set to within $\pm$0.5 degree of the desired values.

CALIBRATION OF THE WIND-SPEED AND -DIRECTION INDICATORS

The wind-speed and -direction indicators which were recorded on the oscillograph were calibrated to check the expressions supplied by the manufacturer.

The wind-direction calibration slope used in data reduction is 59.0 degrees per inch of oscillograph deflection. The associated error is $\pm$6 percent.

The wind-speed calibration supplied by the manufacturer related the meter output in cps to the wind speed in miles per hour,

$$V_f = \omega_{WM}(3.384381) + 0.627 \qquad (2)$$

where

V_f = the indicated velocity in mph

ω_{WM} = the measured output frequency in cps

From calibrations performed in CAL's wind tunnel, Equation (2) yields velocities approximately 2 percent lower than actual, provided the wind speed is greater than 7 feet per second. For wind speeds less than 7 feet per second, the error increases rapidly.

TEST PROCEDURES

The tests were conducted on the main northeast-southwest runway at the Greater Buffalo International Airport, Buffalo, New York. Days on which tests could be conducted were limited by weather and wind conditions. Tests were not conducted unless the local wind speed was less than 3 mph. This requirement generally forced testing to be conducted during the very early morning hours.

Recording instrumentation was allowed at least 4 hours to warm up prior to collecting data. This was required to insure stable operation of the amplifiers. A safety checkout procedure was executed prior to each set of runs.

Atmospheric temperature and pressure were recorded prior to and at the end of each day's running.

Since the most difficult parameter to change was the angle between the thrust axis and the free-stream velocity (τ), this angle was set the day before an anticipated test date and generally not changed until all other parameters had been varied over their entire range. With τ fixed, the blade angle (β_R) was set. The reference blade was placed in a horizontal position and all amplifiers were balanced. A zero reference record was taken. The propeller was then brought to a preselected speed (Ω). Each signal trace was checked to insure that it was neither so large that it was off the paper nor so small as to make its analysis difficult. Any necessary changes in amplifier attenuations were made. Preliminary test condition data were recorded; i.e., indicated prop speed, attenuation settings of all amplifiers, atmospheric pressure and temperature, blade-angle setting, etc. With the prop speed at Ω and no forward speed, a data point was taken. This point constituted a hover point (provided the local wind velocities were negligibly small). Then, holding Ω fixed,

the test facility was accelerated to a predetermined velocity (V_f) and maintained at that speed as long as runway length permitted. Records were taken. At the same Ω , data at several other V_f's were taken.

Then, with τ and β_R held at the same values and the test facility stationary, the next Ω was set and the trace levels were checked. Preliminary test condition data were recorded as was the hover data point. The test facility was again accelerated to the desired V_f and data were taken.

When all the desired prop speed variations had been accomplished, β_R was changed and the same variations in Ω and V_f were performed.

The last variable to be changed was τ . The above procedure was repeated for β_R, Ω, and V_f .

A given Ω and/or V_f was generally repeatable to within $\pm$10 percent.

DATA REDUCTION

Each performance trace was identified and read at 15 equally spaced intervals for one propeller revolution. The values were digitized and fed into a digital computer program. The program performed the operations necessary to convert the trace deflections to loads, to remove the tare values due to prop weight, and to print out the results. The program has the capability of harmonically analyzing the performance data. However, due to the fact that the fundamental and higher harmonics of the performance quantities are seriously affected by the uncertainty associated with the magnitude and character of the calibration matrix (Table I), the harmonically analyzed performance data were not presented. A listing of the program is presented in Appendix II.

The strain data were reduced by reading the mean value of each strain trace and then feeding this digitized value to a digital computer program. The program converted the trace deflections into strains experienced by each gage at each spanwise station. These strains were then combined to yield the principal strains and principal axes. The principal stresses were then computed. The program is capable of harmonically analyzing the strain data also. The strain data reduction program is included in the listing of Appendix II.

EXPERIMENTAL RESULTS

A total of 60 data points was collected. A data point was any combination of V_f , Ω , τ , and β_R at which the prop performance and blade stresses were recorded. The ranges of parameters covered are presented in Table V. For each Ω listed, data were obtained at four values of V_f . The relatively low values of β_R selected were required by the limitation on the available torque from the test facility power plant. The maximum torque theoretically available was 470 foot-pounds. The maximum torque actually obtained during these tests was 360 foot-pounds.

The forward velocity limits were determined by the runway length available and the acceleration limitation of the test facility. Thus, the maximum speed attained was approximately 50 miles per hour.

The accuracy to which the experimental performance data is known varies from component to component. Consider first the thrust component. It is believed that the margin of error associated with the thrust measurement is approximately ± 8 percent. This is due to (i) the ± 5 percent uncertainty in the thrust calibration constant associated with the experimental hysteresis loop, (ii) the questionable magnitude of the coupling terms due to the inplane force and moment in the thrust equation,and finally, (iii) the errors associated with reading the traces. The torque is known to ± 4 percent. The inplane force and moment measurement errors are estimated to lie between 10 percent and 20 percent. This is due largely to the fact that, generally, the inplane loads and moments measured were small compared to the correction necessary to account for the propeller weight component and the large uncertainty associated with the magnitude of the coupling terms. The strain measurements are believed to be accurate to ± 6 percent.

Table V
TEST PARAMETER VALUES

1. $\tau = 0°$		
$\beta_R = 5°$	$\Omega \approx$ 800 rpm	$V_f \approx$ 0 mph
	1380 rpm	13 mph
	1800 rpm	27 mph
		45 mph
2. $\tau = 30°$		
$\beta_R = 5°$	$\Omega \approx$ 800 rpm	$V_f \approx$ 0 mph
	1380 rpm	13 mph
	1800 rpm	27 mph
	rpm	45 mph
$\beta_R = 10°$	$\Omega \approx$ 800 rpm	$V_f \approx$ 0 mph
	1240 rpm	27 mph
3. $\tau = 45°$		
$\beta_R = 5°$	$\Omega \approx$ 800 rpm	$V_f \approx$ 0 mph
	1380 rpm	13 mph
	1800 rpm	27 mph
		45 mph
$\beta_R = 10°$	$\Omega \approx$ 800 rpm	$V_f \approx$ 0 mph
		27 mph
		45 mph
$\beta_R = 15°$	$\Omega \approx$ 800 rpm	$V_f \approx$ 0 mph
		27 mph
		45 mph
4. $\tau = 65°$		
$\beta_R = 5°$	$\Omega \approx$ 800 rpm	$V_f \approx$ 0 mph
	1380 rpm	13 mph
	1800 rpm	27 mph
		45 mph
$\beta_R = 10°$	$\Omega \approx$ 1380 rpm	$V_f \approx$ 0 mph
		23 mph

In addition to the error in the wind-speed measurement discussed previously, there existed an error in this measurement due to flow induced by the propeller. For the hovering and very low forward speeds, the velocity induced by the propeller at the location of the anemometer was not negligible. A correction to the measured airspeed based on the induced flow field predicted in Reference 4 was made. At speeds in excess of 30 feet per second, the correction was negligible and the wind speed measured was used. It is estimated that for speeds greater than 7 feet per second, the error in the measured wind velocity is ± 7 percent. At speeds less than 7 feet per second, the error may be as high as 20 percent.

Plotted in Figures 9 through 16 are the values of the experimental performance characteristics versus free-stream velocity for several values of τ and β_R. Indicated on each curve are the experimental values, the associated error band, and the measured propeller speed (Ω). Curves were faired through experimental points for which Ω did not deviate by more than ± 5 percent from the mean.

The thrust versus V_f curves generally indicate that, as the velocity is increased, the thrust output decreases. This appears to be true for any Ω, β_R, or τ with the exception of $\tau = 65$ degrees (Figures 15 and 16). For this τ, the curves indicate an increase in thrust to some value of V_f, and thereafter, a decrease in thrust for further increases in V_f. The peak or maximum thrust depends upon the prop speed. Note that for the very low values of Ω and relatively high V_f, the thrust curve became negative for all values of τ except $\tau = 65$ degrees. For approximately the same Ω, the thrust curve became negative at higher values of V_f as τ increased. The thrust curves moved to higher values almost parallel to themselves as Ω was increased.

Increasing forward velocity for a fixed Ω did not seem to affect the required torque (Q) over the velocity range tested. The torque curves (Q vs V_f) moved to higher values almost parallel to themselves as Ω was increased.

While the variation of both the T and Q curves was smooth and generally decreased slightly as V_f increased for all values of Ω, τ, and β_R, this was not the case with the inplane force and moment curves. The inplane force was plotted in terms of its components: normal force (NF) and side force (SF). The inplane moment was plotted in terms of its components: pitching moment (PM) and yawing moment (YM).

In Figure 9 (c-f), the variation of the inplane force and moment components is plotted versus V_f for β_R = 5 degrees and τ = 0 degrees. This corresponds to axial flight. For the configurations tested, no inplane force or moment was expected due to aerodynamic loading. However, variations with V_f and Ω were observed in all components. The components observed might be attributed to:

(i) Aerodynamic forces and moments generated by the hub and pitch-change mechanism.

(ii) Aerodynamic interference effects from the pod and tower.

(iii) Deviation from a true axial flight condition.

The characteristics of the NF and SF curves continue to behave in a peculiar fashion as τ is increased (Figures 10 through 16). The PM and YM curves, however, seem to indicate definite trends. With the exception of the curves for $\Omega \approx$ 1380 rpm (τ = 30 degrees and β_R = 5 degrees), $\Omega \approx$ 1440 rpm, and Ω = 880 rpm (τ = 45 degrees and β_R = 5 degrees), the PM decreases as V_f increases for all values of Ω and τ. The same comment appears to be applicable for β_R = 10 degrees and β_R = 15 degrees (see Figures 11, 13, 14, and 16). The behavior of PM with Ω is not clear.

With the exception of axial flight, the behavior of YM with V_f for all Ω, τ, and β_R is to increase as V_f increases to some value, and then decrease as V_f is further increased. For any given τ other than 0 degree (β_R fixed at 5 degrees) and V_f, an increase in Ω

increases YM. Further, as τ is increased, the YM is increased for any given V_f and Ω (β_R again fixed at 5 degrees).

From the data of Figures 9 through 16, cross plots were made to indicate trends with Ω, τ, and β_R. Figures 17 through 20 are plots of T and Q versus the average prop speed noted on Figures 9 through 16. The plots are presented for β_R = 5 degrees only and for various values of V_f and τ. Again, the T and Q are generally smooth, well-behaved curves showing an increase in both thrust output and torque required as Ω is increased for any specified τ and V_f.

Figure 21 is a plot of T and Q versus τ for β_R = 5 degrees. Shown is the variation of T and Q for two prop speeds and two velocities representing the upper and lower experimental bounds of these variables. It is noted that as τ is increased from 0 degree, the thrust increases to a maximum at some value of τ. The value of τ at which this maximum occurs is dependent upon V_f and Ω. As τ is increased further, the thrust begins to decrease.

The variation of the required torque is more complex. As τ is increased to approximately 15 degrees, the required torque increases to a maximum. A further increase in τ to approximately 50 degrees results in a decrease in torque. Finally, indications are that, as τ is increased beyond 50 degrees, the torque will begin to increase again.

For a τ = 45 degrees, Ω = 822 rpm, and V_f = 40 feet per second, Figure 22 shows that both T and Q increase at an increasing rate as β_R is increased from 5 degrees to 15 degrees.

Because of the low blade angles at which these tests were run and because negative thrusts were obtained for several test conditions, it was conjectured that the propeller was being operated in a range in which its efficiency was very low. To substantiate this conjecture, the

results from the axial flight case were plotted as C_T, C_P, and η versus J where

C_T = thrust coefficient = $T/\rho n^2 D^4$ (3)

C_P = power coefficient = $2\pi Q/\rho n^2 D^5$ (4)

η = efficiency = $(C_T/C_P)J$ (5)

J = advance ratio = V_f/nD (6)

ρ = density — slugs/ft^3

D = prop diameter — ft

n = prop speed — cps

Presented in Figure 23 are C_T, C_P, and η versus J based on the data collected. From the η versus J curve, it is apparent that at β_R = 5 degrees the prop is very inefficient.

Plotted in Figures 24 through 27 are the measured longitudinal stresses versus span for the various Ω's and V_f's at which tests were conducted. The strain measurements from which these stresses were computed were measured on the top or camber side of the blade. Positive stress indicates tension. As expected, it was found that the stress level usually decreased as the spanwise position increased. The stress level at a given spanwise position generally increased as Ω increased. Further, for a given Ω as V_f increased, the stress level increased. This is attributed to the fact that as V_f increased, the thrust, or lift per blade, decreased. The decreased blade load reduces the compression load induced in the fibers on the blade camber (atop) surface. Thus, the rotation-induced tensile load is reduced by a smaller amount and the entire longitudinal stress increased.

Figure 24 presents the results for τ = 0 degree. For $\Omega \approx$ 850 rpm, the load distribution is such that the observed longitudinal stress becomes negative at the 3.5-foot radius for all forward velocities. (The two curves designated by τ = 0 degree, β_R = 5 degrees, Ω = 873 rpm, and V_f = 16 miles per hour were run under the same test conditions to determine repeatability.) The reason for this peculiar distribution of the stress curve is unknown. As Ω is increased, the tensile stress curves become smoother and are positive at all spanwise locations except for the case at $\Omega \approx$ 1500 rpm and V_f = 46 miles per hour.

A similar behavior is observed in Figure 25 where the primary change has been in τ (τ is now 30 degrees). The behavior of the stress curve with Ω and V_f is substantially the same as at τ = 0 degree. An increase in β_R from 5 degrees to 10 degrees results in a marked decrease in stress level for the same Ω and V_f. This is again attributed to the increased load generating increased compression loads due to bending in the upper fibers of the blade. Note that the unusual behavior at Ω = 850 rpm disappeared at β_R = 10 degrees.

The results for τ = 45 degrees are presented in Figure 26. For β_R = 5 degrees, the effect of V_f on the stress was not as pronounced as for τ = 0 degree and 30 degrees. However, as β_R increased to 10 degrees and 15 degrees, the effect of V_f became larger. Note again the marked decrease in blade stress on the camber face as β_R is increased.

Figure 27 presents the results for τ = 65 degrees. The free-stream velocity has almost no effect on the stress level for β_R = 5 degrees at this τ.

COMPARISONS OF THE EXPERIMENTAL DATA WITH THEORETICAL PREDICTIONS AND OTHER EXPERIMENTAL DATA

An attempt was made to compare the data obtained in the current tests with the results presented in Reference 5. The tests in Reference 5 were performed in the NASA Ames 40-foot by 80-foot wind tunnel on three propellers having three blades each. The planforms were different from one another as well as being different from the blade planform used in the current tests. However, since the trends reported were much the same for all the propellers tested in Reference 5, it was felt that the propeller tests of this report should yield similar trends.

The results of Reference 5 were presented as plots of C_T and C_P versus J' at various β_R and τ. The parameter J' was defined as

$$J' = V_f \cos\tau / nD \quad \text{(Modified Advance Ratio)}, \quad (7)$$

It was not noted whether the J' variation was obtained by varying V_f and holding Ω constant, or by varying Ω and holding V_f constant, or by allowing both V_f and Ω to vary. Cross plots were made of C_T and C_P versus τ at constant values of J'. One of the conclusions drawn was that "C_T and C_P for given values of β_R and J' are nearly constant in magnitude over a large range of τ and that range diminishes with increasing J'".

The data presented in Figures 9, 10, 12, and 15 were put in coefficient (C_T, C_P) form and J' was computed for each point. The curves are presented in Figure 28. The solid curves were obtained holding Ω constant; the dotted curves were obtained holding V_f constant. Thus, the character of the C_T and C_P versus J' curves apparently depends upon the manner in which the data were generated. Further, if cross plots of C_T and C_P versus τ at any specified J'

were made from either the V_f = constant or Ω = constant curves, the curves would not be constant with τ over any range of τ. These results seem to be in contradiction to the results obtained in Reference 5. No reasons for these results could be found in the data collected.

Thus, from the data collected by CAL, it would appear that J' is not an independent parameter in the problem of a propeller operating in transitional flight.

The theoretical computer program developed by CAL (Reference 1) was run for five different cases for the purpose of correlation. The variables associated with said cases are presented in Table VI. The mean values of the performance for each case were plotted in Figures 9, 11, 12, 14, and 16. The theoretical points are indicated by a symbol with a flag.

Table VI
VALUES OF PARAMETERS USED IN THEORETICAL CALCULATIONS

IDENTIFICATION	τ deg	β deg	Ω rpm	V_f mph
CASE 1	0	5	1875	50
CASE 2	30	10	1277	32
CASE 3	45	5	819	31
CASE 4	45	15	834	29
CASE 5	65	10	1428	37

The axial flight results of Figure 9 indicate that the predicted T is 111 percent too high while the predicted Q is 27.9 percent too low. The reason for this very large discrepancy in thrust is attributed to the fact that the propeller was operating very nearly in a windmill brake state. The theoretical results indicated that the outboard

20 percent of the blade was operating at negative values of lift. This operating condition causes computational errors in the theory. First, the lifts which result from negative effective angles of attack are in error. In the negative angle-of-attack range, the two-dimensional airfoil characteristics were programmed to be simply straight-line extrapolations from their values at zero angle of attack. This approximation becomes progressively poorer as the angle of attack becomes more and more negative. The error is such as to predict a larger local lift so long as the lift is positive. When the lift becomes negative, the error is such as to predict a smaller local lift. Second, the fact that the distribution of the bound vorticity is such that it passes through zero three times (once at tip, root, and one intermediate spanwise location) presents difficulties in assigning the proper strength and position to the trailing tip and root vortices employed in the mathematical model of the rolled-up wake. Indeed, a more reasonable rolled-up wake representation for a blade having such a distribution would be two pairs of vortices.

The inplane forces and moments predicted by the theory for the axial flight case are zero. As noted before, the cause of the experimentally obtained forces and moments is unknown.

The transition Case 2 results are plotted in Figure 11. The predicted thrust is 15 percent higher and the torque is 13 percent higher than the corresponding experimental values. The values of NF, SF, and PM are underpredicted while YM is overpredicted.

In Figure 12, the results for transition Case 3 are presented. The thrust was overpredicted by approximately 17 percent and the torque underpredicted by 25 percent. For this case, the theoretical NF and PM are less than the corresponding experimental values, while the theoretical SF and YM are greater than the experimental values.

For transition Case 5 (Figure 16), the theoretical thrust is 20 percent higher and the theoretical torque is approximately 40 percent higher. Again, correlation with the inplane moments and forces is poor.

During the theoretical investigation of Case 5, it was discovered that the magnitude and position of the tip vortex representing the rolled-up wake played a significant role in the prediction of the thrust and torque. This was found to be so even though the wake model was such that the effect of a mesh of trailing and shed vorticity was included in the computation for 180 degrees of blade azimuth prior to rolling up into a concentrated tip and root vortex. It was found that increasing the magnitude of the rolled-up tip vortex by 20 percent and shifting its spanwise position in the wake from the 93-percent span to the 50-percent span caused a 10-percent reduction in the predicted thrust and a 5-percent reduction in the torque.

In these transition cases, it was noted that the predicted effective angle of attack (α_e) was generally very small and resulted from the differences between the built-in twist, β , the induced angle of attack, α_I , and the live twist, θ ; i. e., at any station

$$\alpha_{e_j} = \left[\beta - \alpha_I + \theta\right]_j \qquad j = \text{station number.} \tag{8}$$

For those cases in which $\beta \simeq \alpha_I$, the magnitude of θ plays a very important role in determining the blade loading. Thus, a relatively small error in the predicted θ distribution could result in a relatively large error in the predicted propeller performance.

In an attempt to support the above arguments, calculations for Case 4 were performed. This case was selected because it was believed that the final effective angles of attack would be sufficiently large, positive quantities that the errors associated with both negative angles and prediction of the torsional deformation would be minimized. The results are presented in Figure 14. Agreement

between the theoretical and experimental values of most of the performance quantities appears to be much improved over the previously discussed cases. The thrust predicted is within the estimated experimental error associated with the measurement. The torque is overpredicted by approximately 23 percent.

The poor correlation obtained for the previously discussed cases may also be attributable to the following:

(i) Inaccuracies in setting the blade angle, β_R . Calculations indicate that, at β_R = 5 degrees, a 10-percent reduction in β_R results in a 21-percent reduction in T and a 15-percent reduction in Q. It is believed that similar variations would be obtained at higher β_R's.

(ii) The use of two-dimensional airfoil data in the analysis. No experimental proof is yet available to answer the fundamental question of whether the use of two-dimensional airfoil section data is reasonable for the propeller.

(iii) The possibility that the errors in the experimental data presented are larger than estimated.

(iv) In a digital program of the complexity of the one developed in Reference 1 and employed here for the purpose of correlation, the possibility for program errors always exists. Though the program has been thoroughly checked, the unusual blade load distributions predicted for the cases computed may have caused the program to operate in an erroneous mode heretofore undiscovered.

CONCLUSIONS

Based on the results obtained in this study, the following conclusions were drawn:

(i) For the range of parameters tested, the quantity $J' = V_f \cos\tau / nD$ is not an independent parameter of a propeller operating in transitional flight.

(ii) As τ is increased from 0 degree, the thrust increases to a maximum at some τ, dependent upon V_f and Ω, and then decreases as τ is increased further.

(iii) As τ is increased from 0 degree, the required torque increases until τ reaches approximately 15 degrees. A further increase in τ to approximately 50 degrees results in a decrease in torque. The required torque begins to increase again as τ is increased beyond 50 degrees.

(iv) The effect of increasing forward velocity, all other parameters held constant, is to decrease the thrust output while the required torque remains essentially constant.

(v) The thrust and torque both increase with an increase in prop speed.

(vi) Both the thrust and torque increase as the blade angle of attack is increased.

(vii) When the propeller was operating in a flight condition for which the theory was developed, correlation between theory and experiment was good.

(viii) Accurate prediction of the blade torsional deflection plays a very important role in determining the blade loadings accurately.

(ix) The position and magnitude of the rolled-up tip vortex must be predicted accurately in order that the thrust and torque may be predicted to within the accuracies required for V/STOL-type propellers throughout the entire flight range.

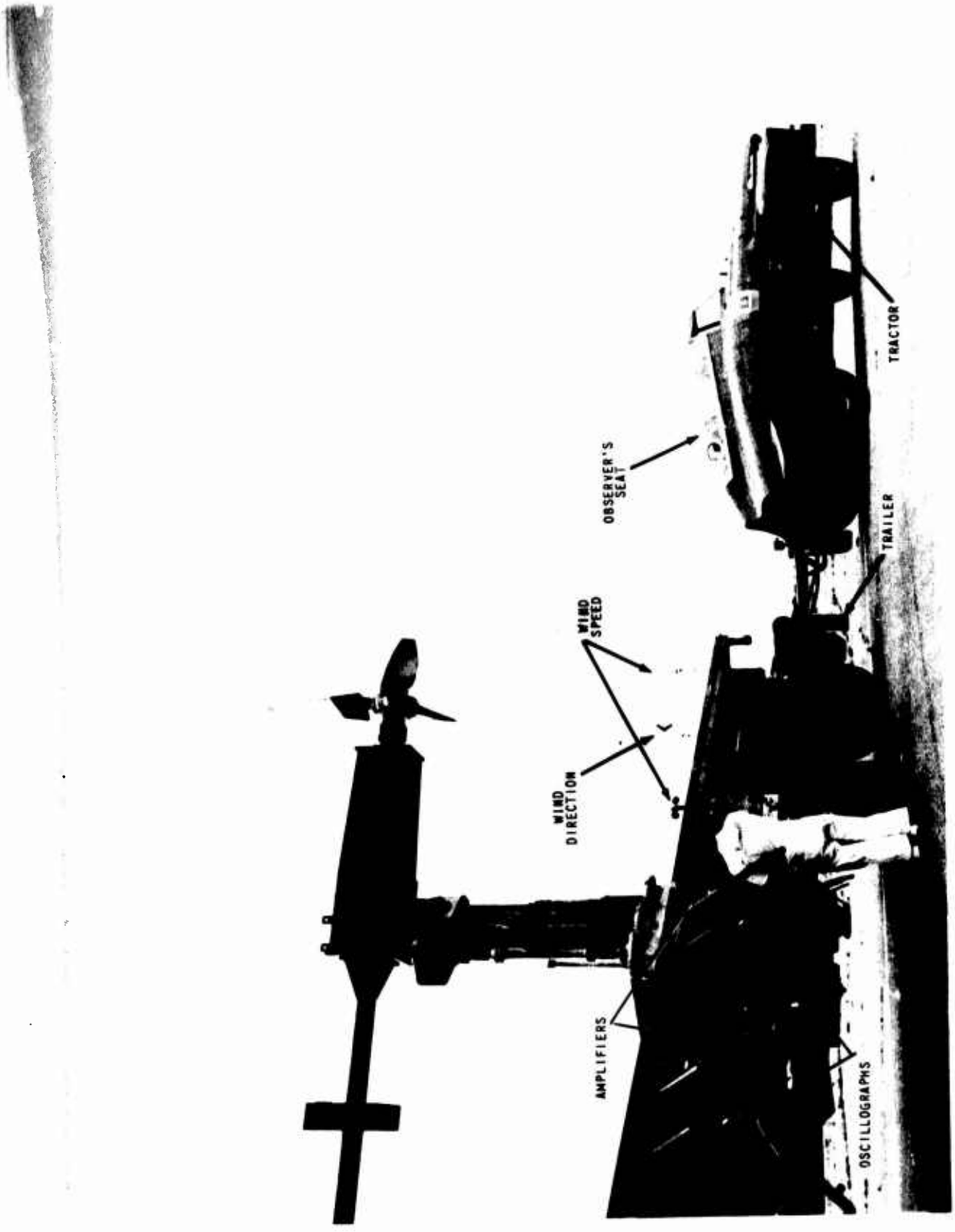

Figure 1. SMALL ROTOR TEST FACILITY.

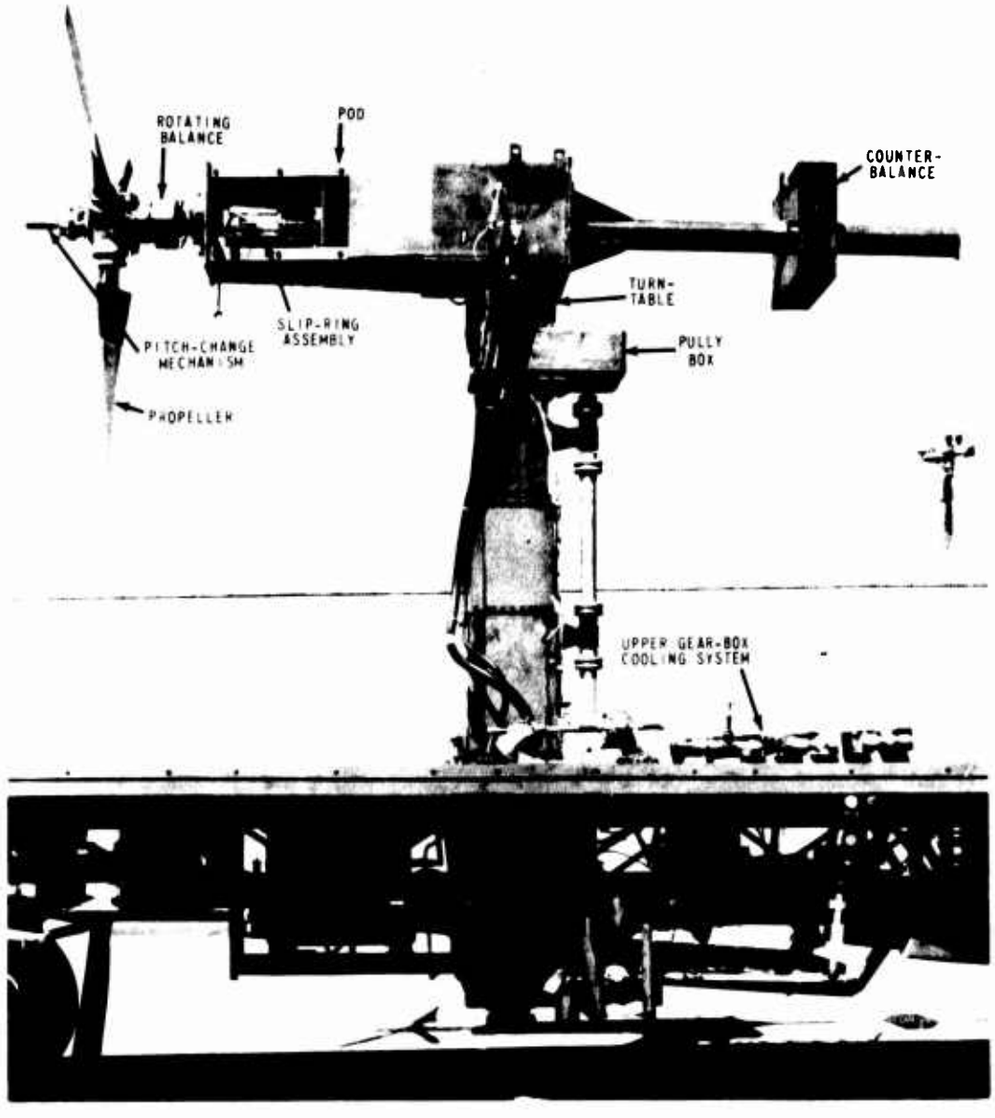

Figure 2. TRAILER-TOWER AND POD ASSEMBLY WITH PROPELLER.

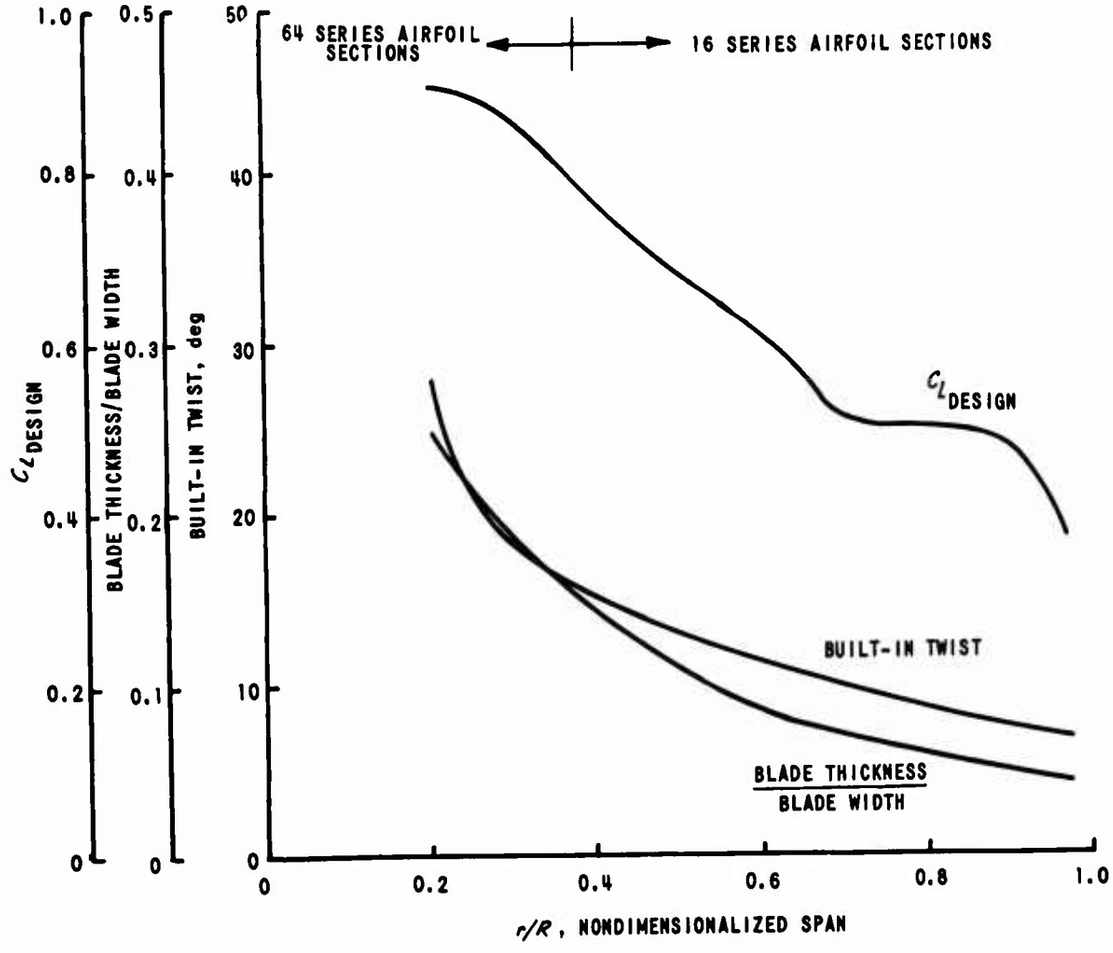

Figure 3. PROPELLER BLADE CHARACTERISTICS.

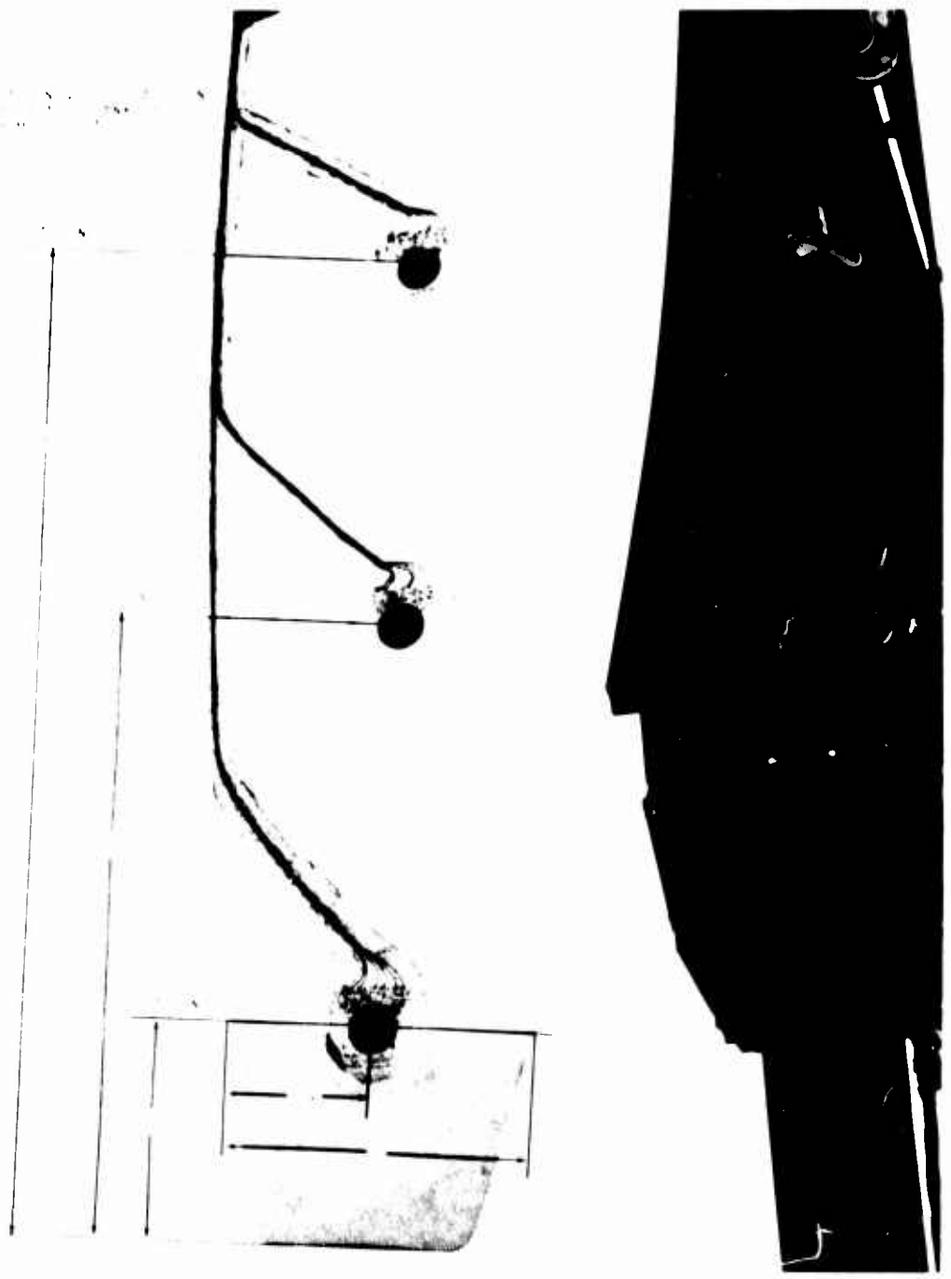

Figure 4. LOCATION OF STRAIN-GAGE ROSETTES.

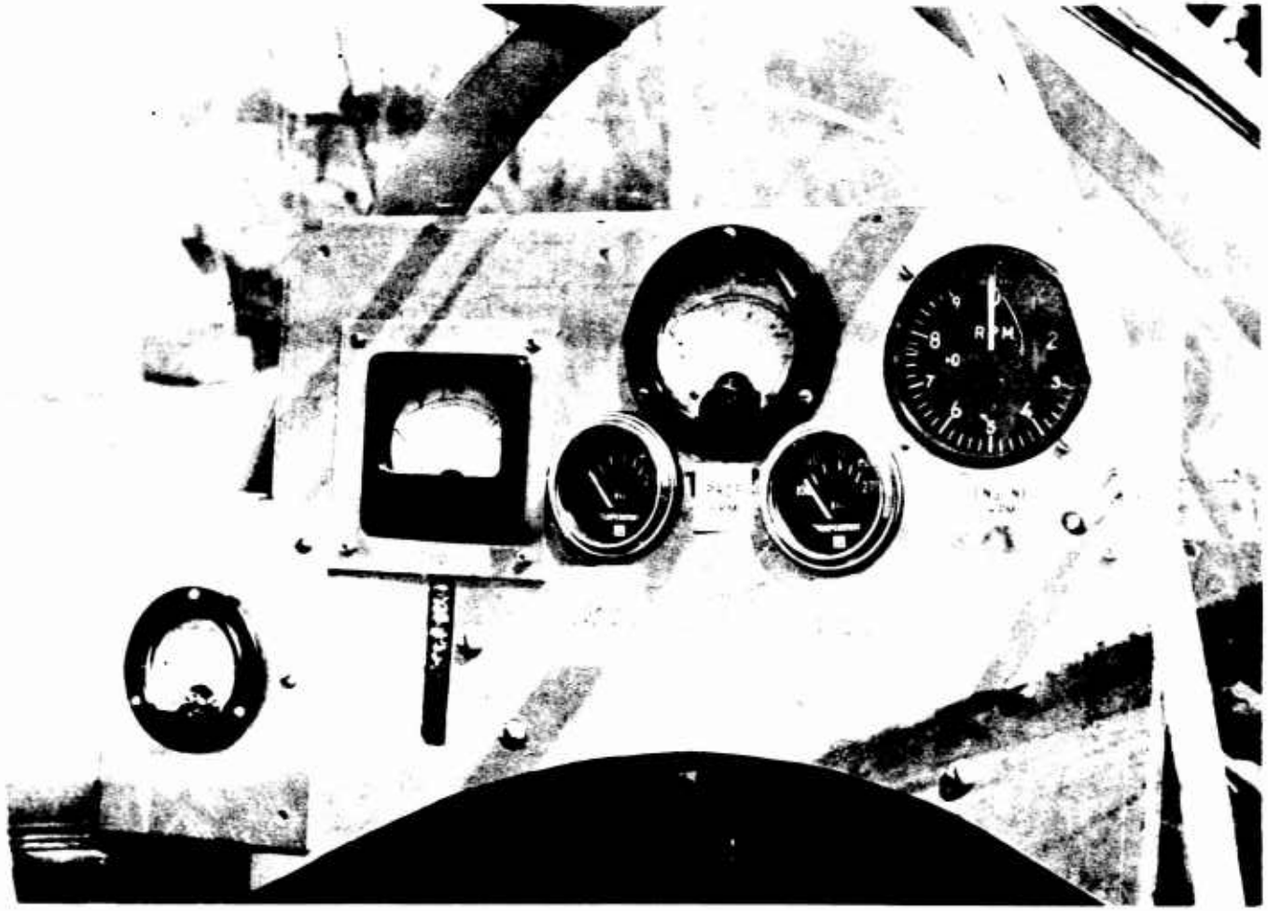

Figure 5. DISPLAY PANEL IN OBSERVER'S POST.

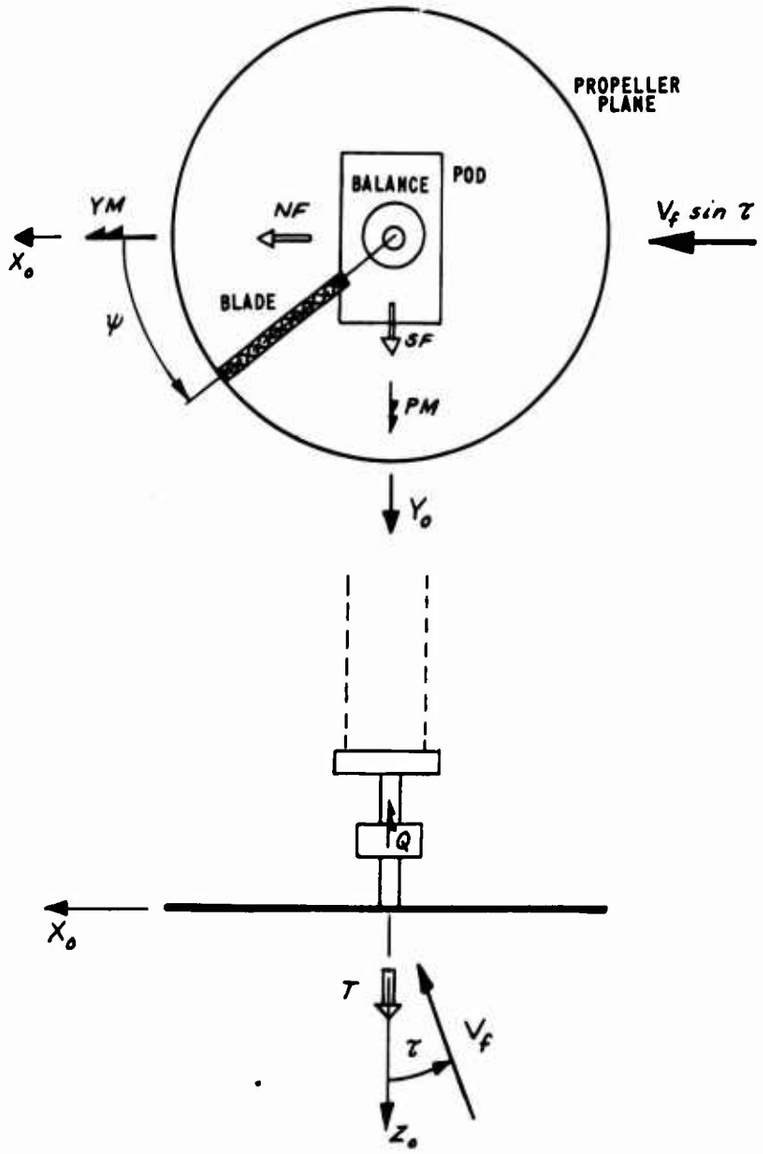

Figure 6. SCHEMATIC OF PROPELLER PLANE AND POSITIVE SHAFT LOADS.

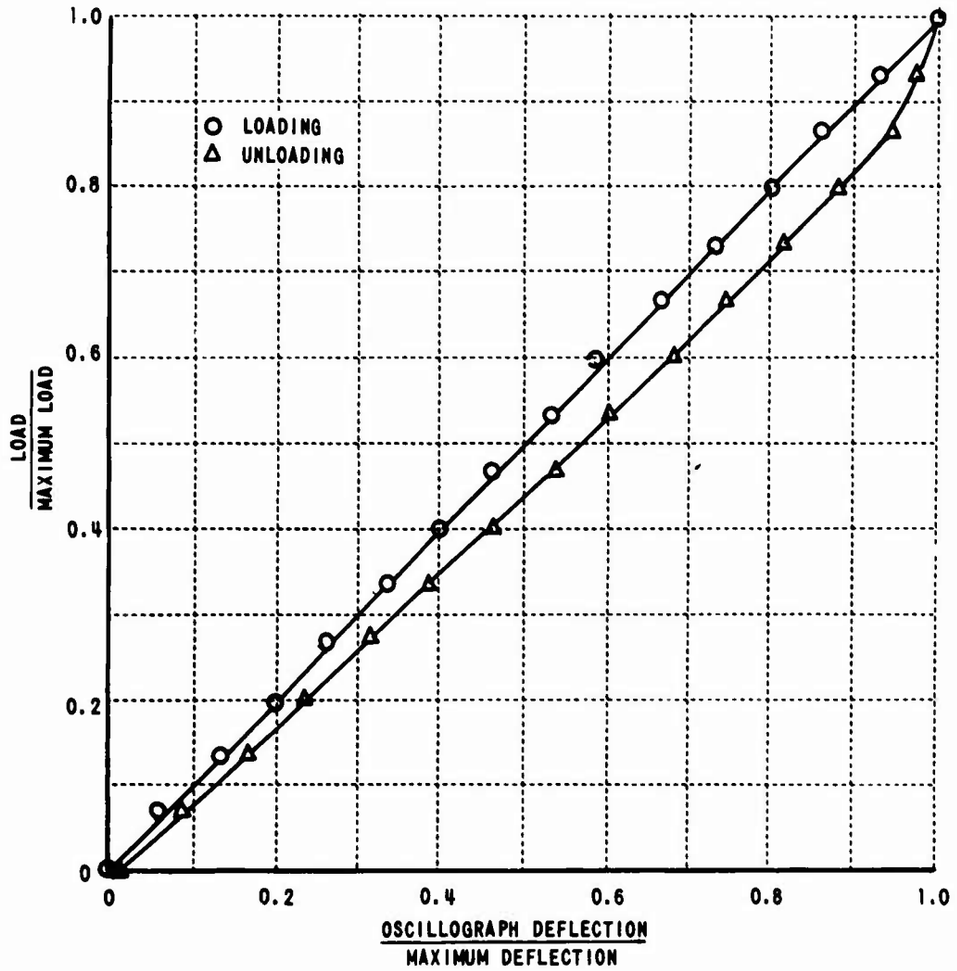

Figure 7. STATIC CALIBRATION CURVE FOR THRUST.

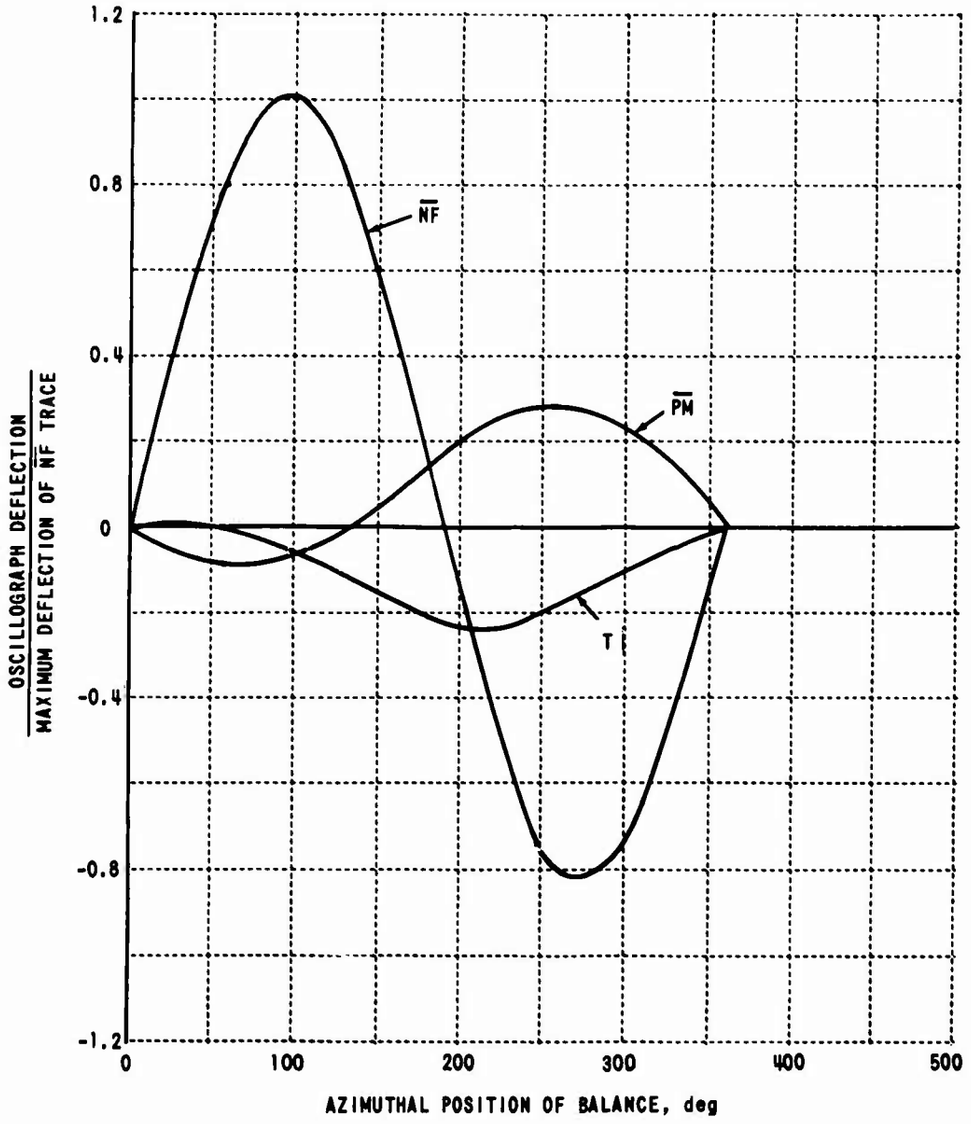

Figure 8. QUASI-STATIC THRUST CALIBRATION RESULTS.

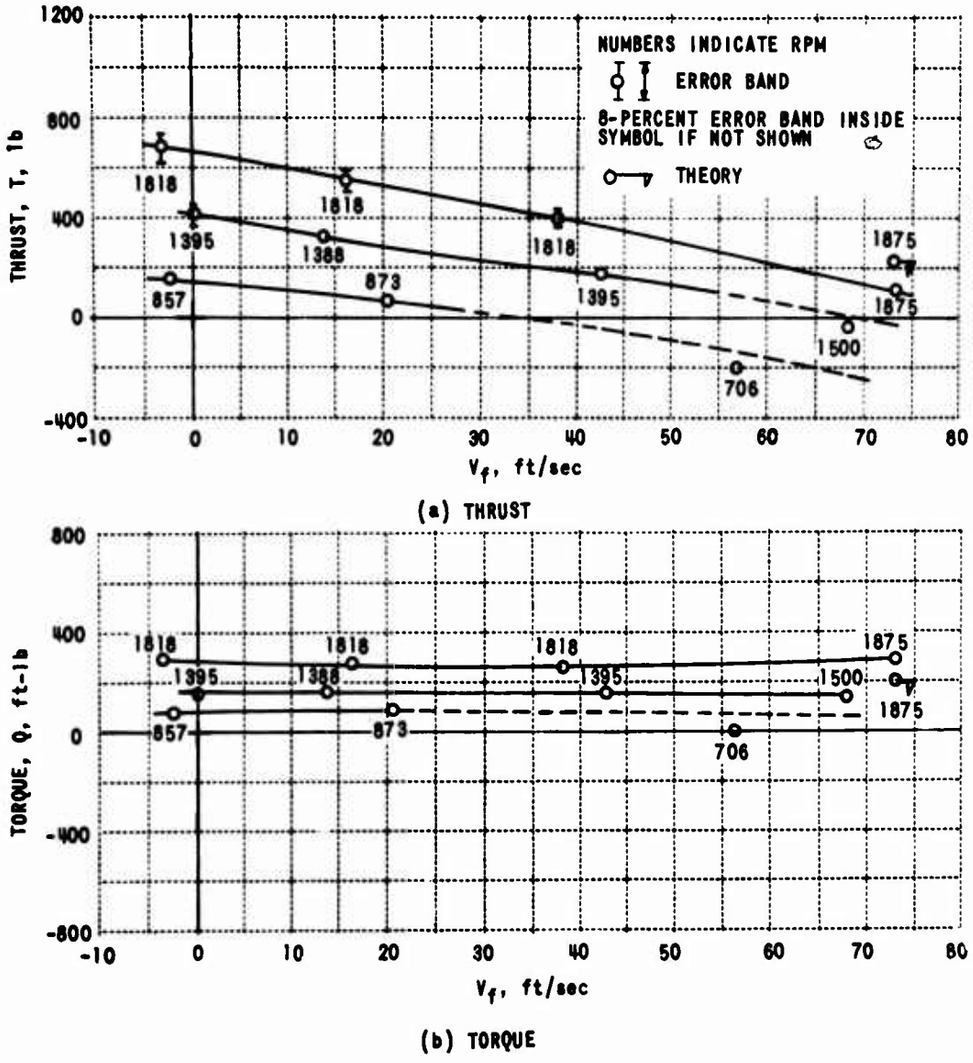

Figure 9. PLOT OF EXPERIMENTAL PERFORMANCE CHARACTERISTICS (T,Q,NF,SF,PM,YM) VS. FREE-STREAM VELOCITY FOR $\tau = 0°$ AND $\beta_R = 5°$.

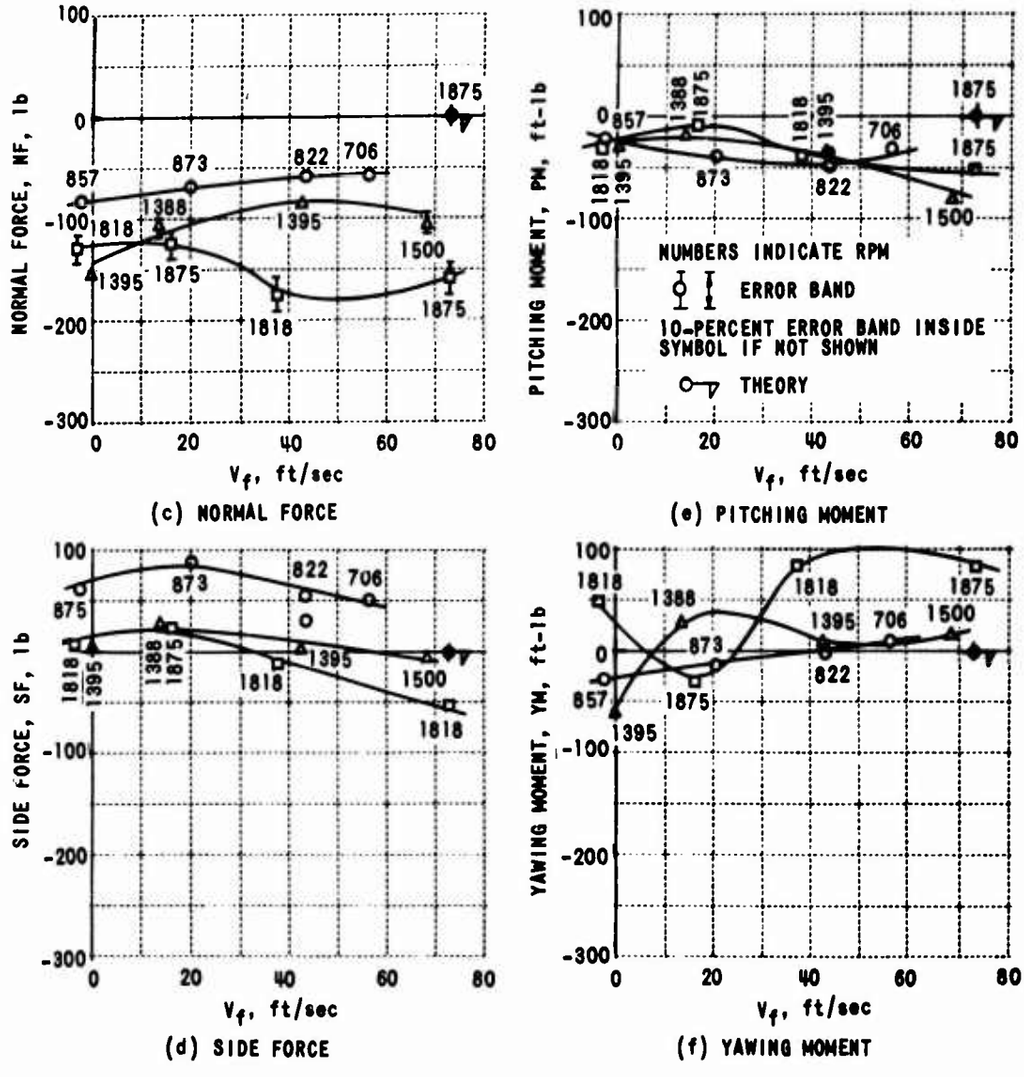

Figure 9 PLOT OF EXPERIMENTAL PERFORMANCE CHARACTERISTICS (T,Q,NF,SF,PM,YM) VS. FREE-STREAM VELOCITY FOR $\tau = 0°$ AND $\beta_R = 5°$. (CONTINUED)

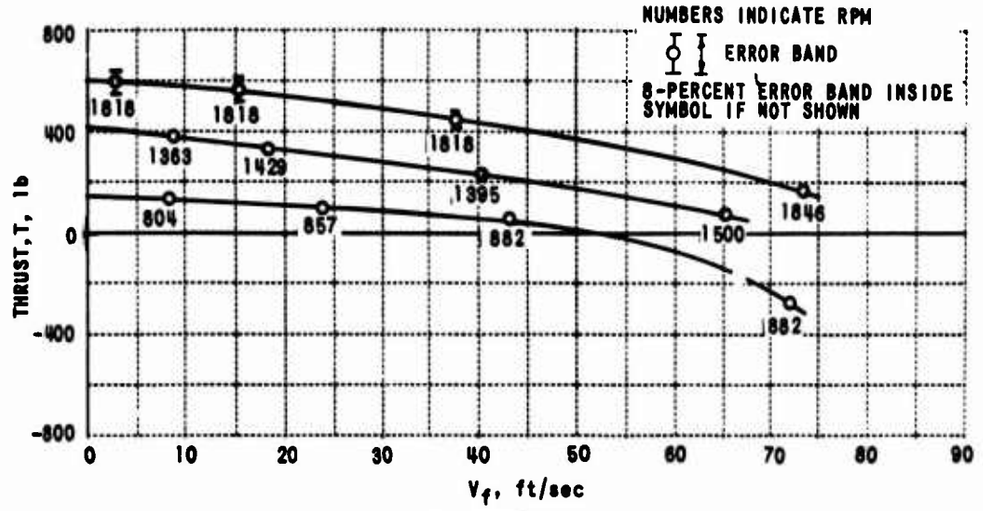

(a) THRUST

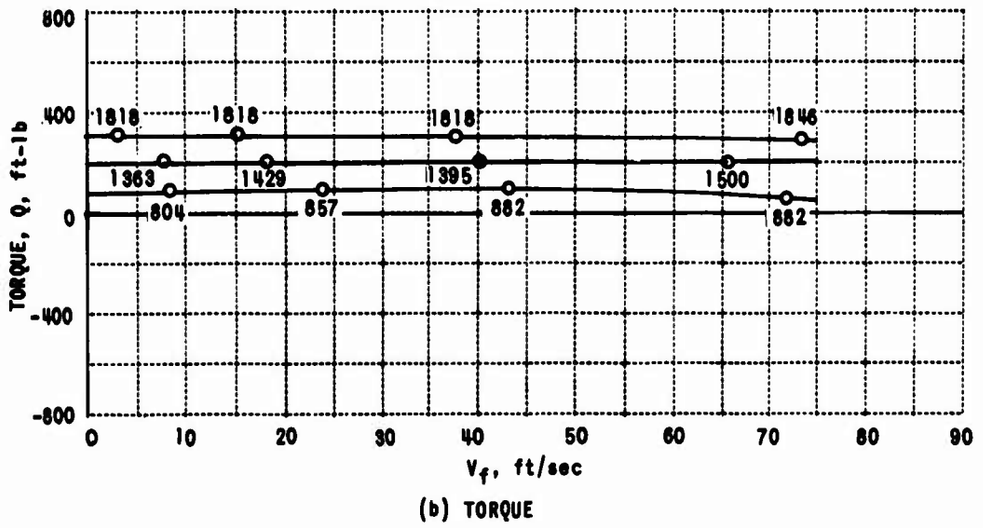

(b) TORQUE

Figure 10. PLOT OF EXPERIMENTAL PERFORMANCE CHARACTERISTICS (T,Q,NF,SF,PM,YM) VS. FREE-STREAM VELOCITY FOR $\tau = 30°$ AND $\beta_R = 5°$.

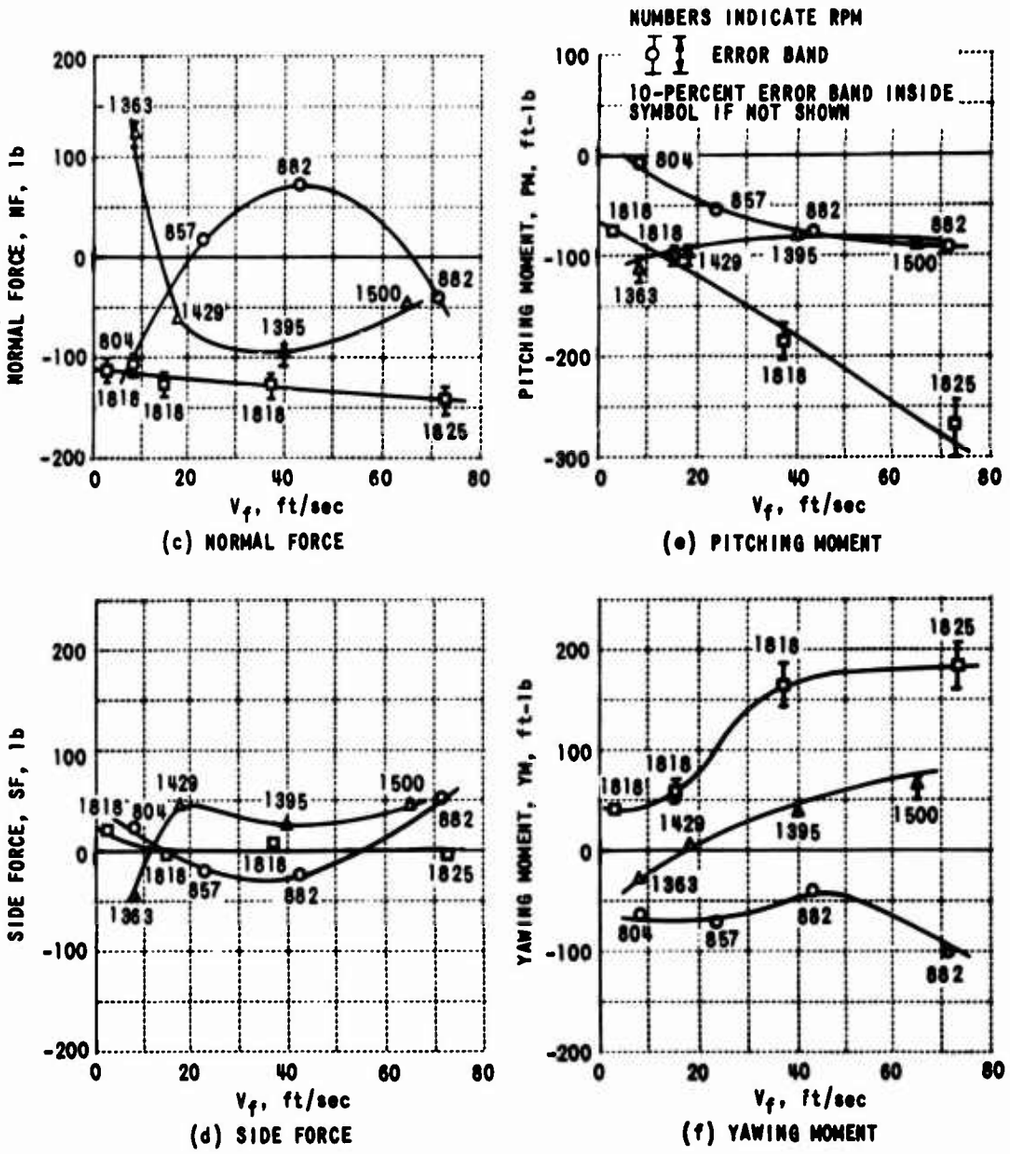

Figure 10. PLOT OF EXPERIMENTAL PERFORMANCE CHARACTERISTICS (T,Q,NF,SF,PM,YM) VS. FREE-STREAM VELOCITY FOR τ = 30° AND β_R = 5°. (CONTINUED)

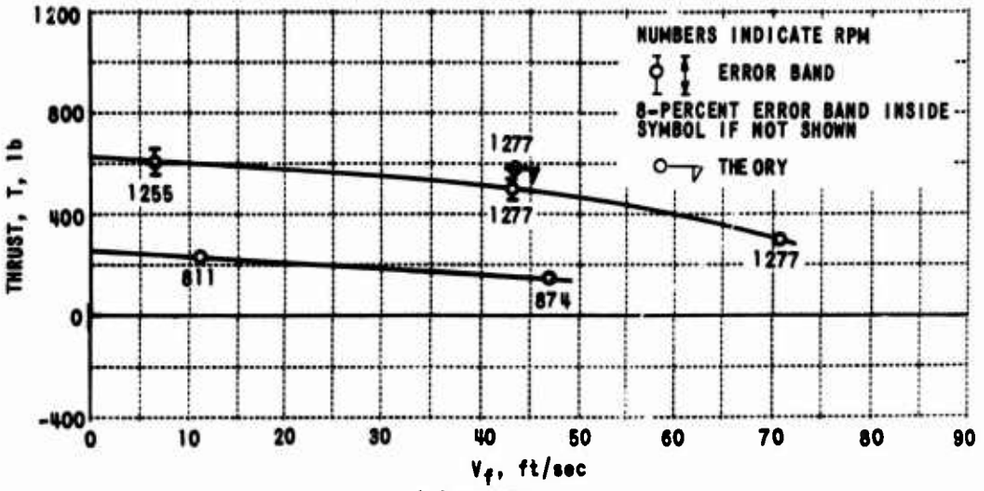

(a) THRUST

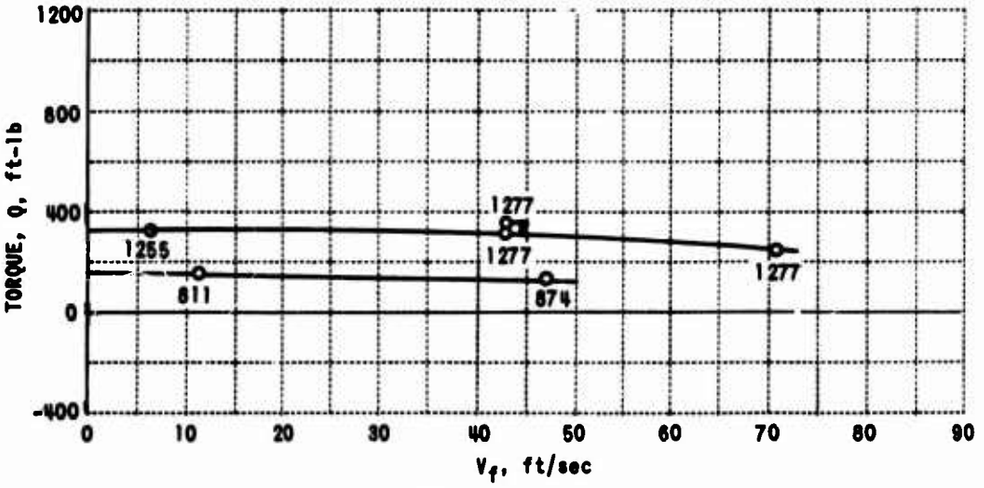

(b) TORQUE

Figure 11. PLOT OF EXPERIMENTAL PERFORMANCE CHARACTERISTICS (T,Q,NF,SF,PM,YM) VS. FREE-STREAM VELOCITY FOR $\tau = 30°$ AND $\beta_R = 10°$.

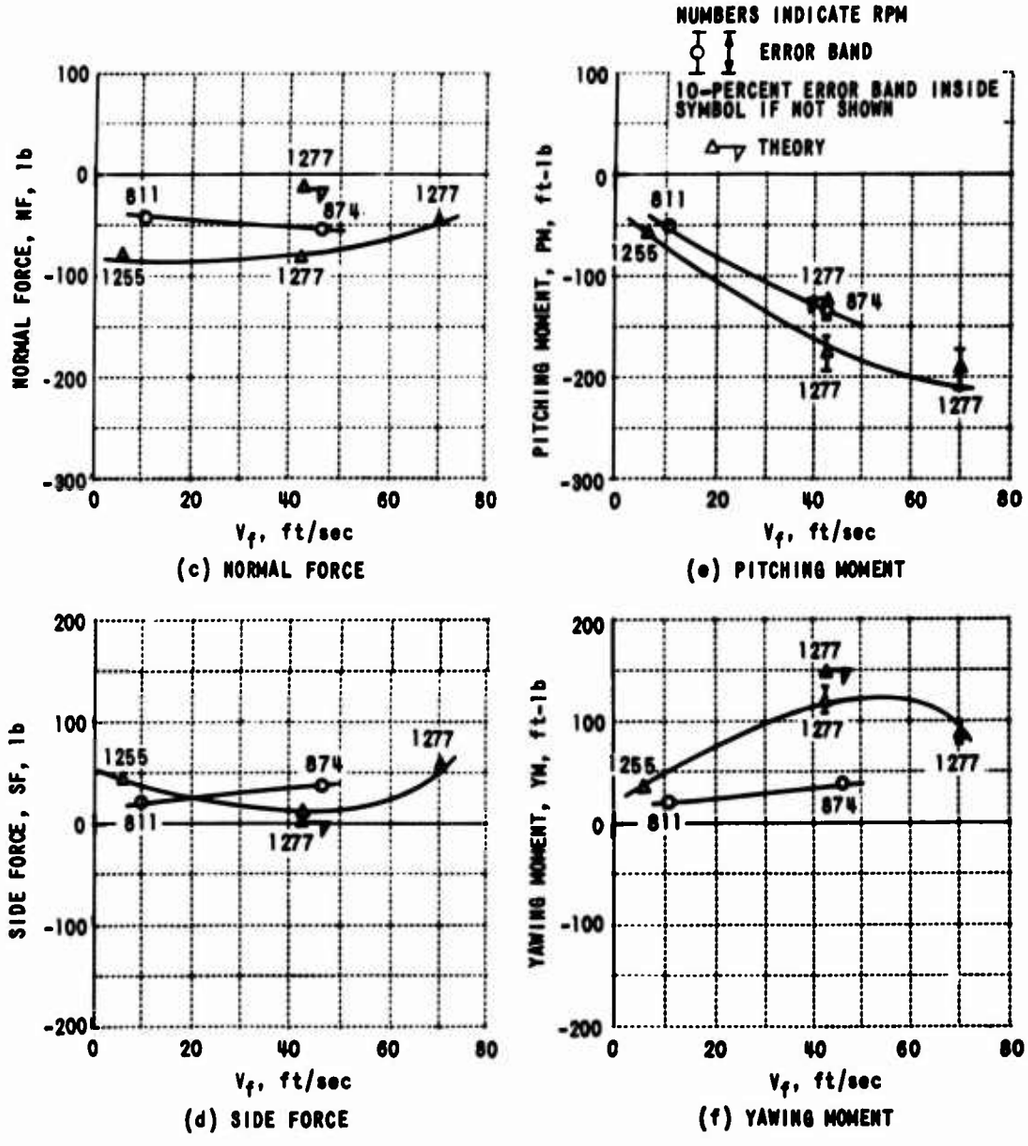

Figure 11. PLOT OF EXPERIMENTAL PERFORMANCE CHARACTERISTICS (T,Q,NF,SF,PM,YM) VS. FREE-STREAM VELOCITY FOR τ = 30° AND β_R = 10°. (CONTINUED)

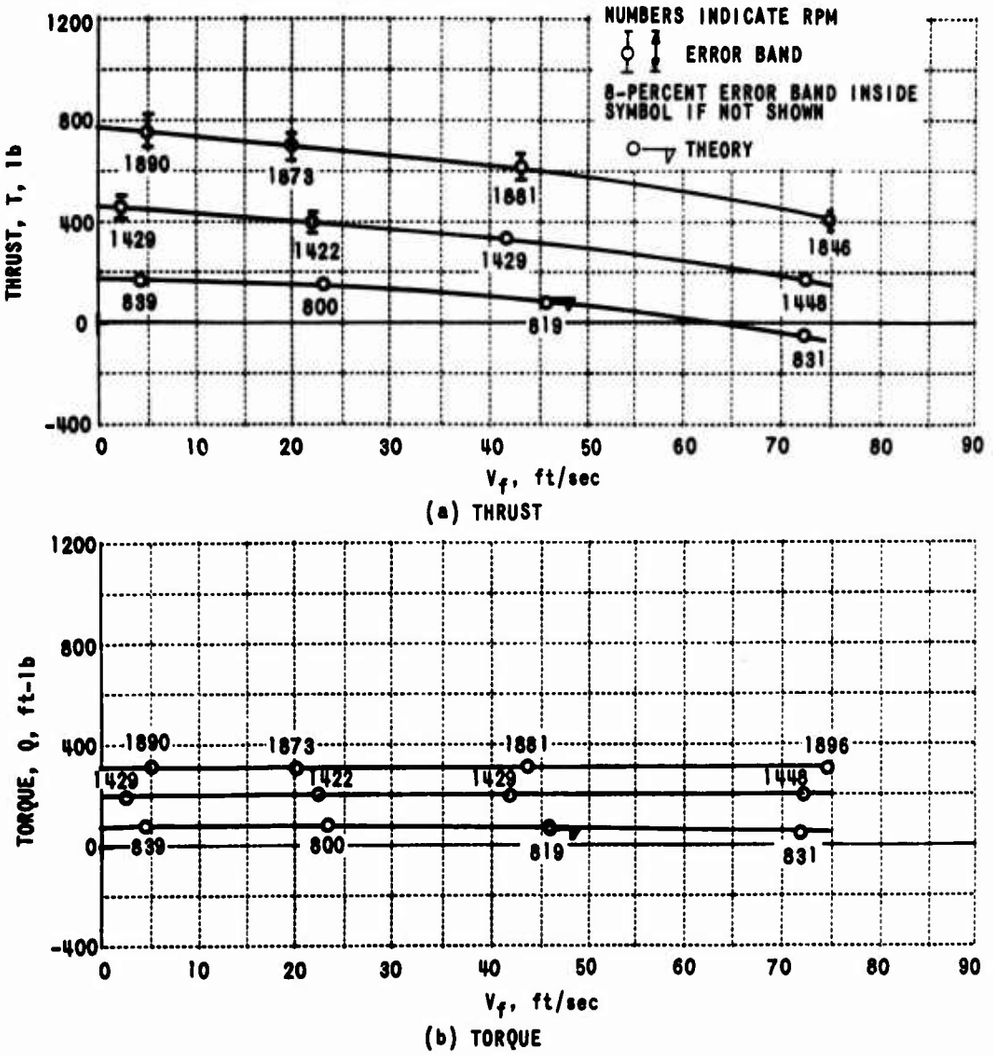

Figure 12. PLOT OF EXPERIMENTAL PERFORMANCE CHARACTERISTICS (T,Q,NF,SF,PM,YM) VS. FREE-STREAM VELOCITY FOR $\tau = 45°$ AND $\beta_R = 5°$.

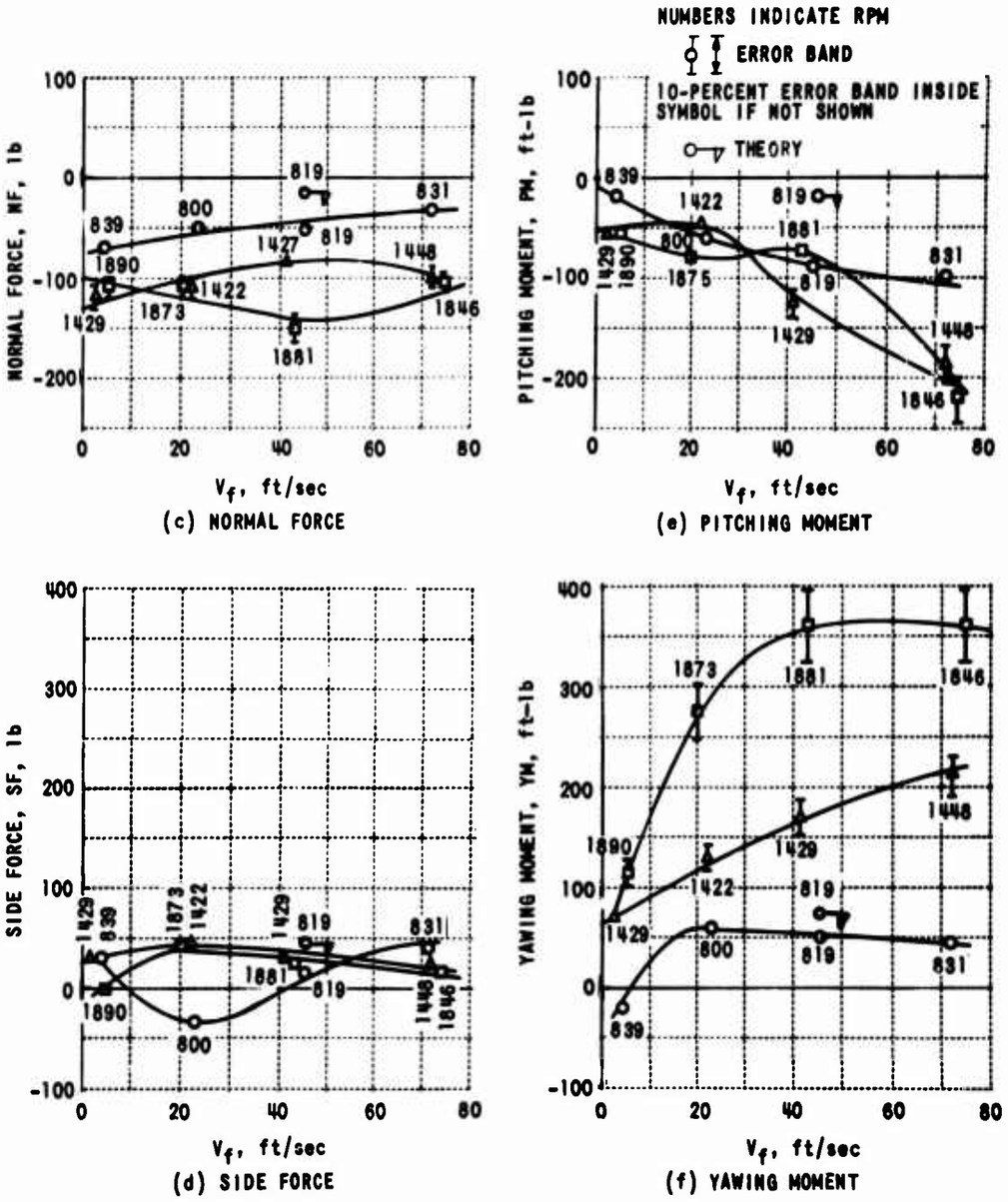

Figure 12. PLOT OF EXPERIMENTAL PERFORMANCE CHARACTERISTICS (T,Q,NF,SF,PM,YM) VS. FREE-STREAM VELOCITY FOR τ = 45° AND β_R = 5°. (CONTINUED)

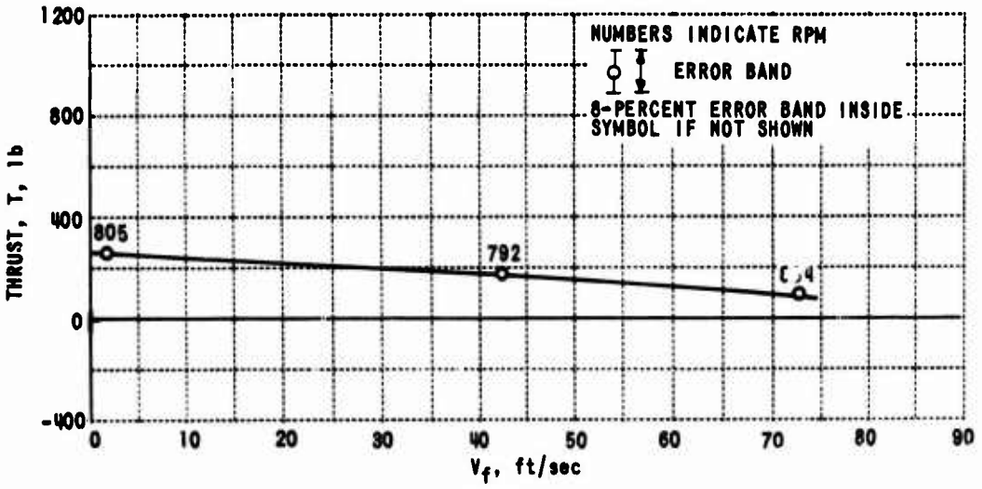

(a) THRUST

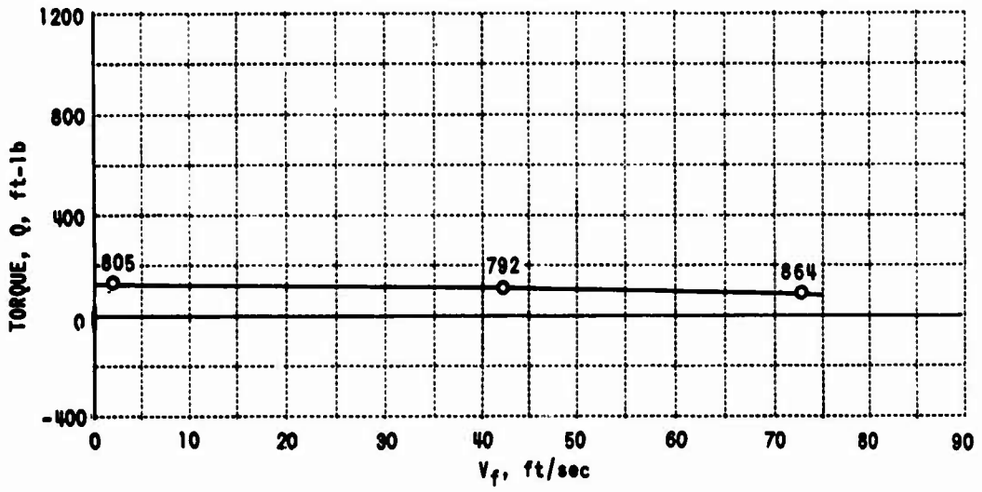

(b) TORQUE

Figure 13. PLOT OF EXPERIMENTAL PERFORMANCE CHARACTERISTICS (T,Q,NF,SF,PM,YM) VS. FREE-STREAM VELOCITY FOR τ = 45° AND β_R = 10°.

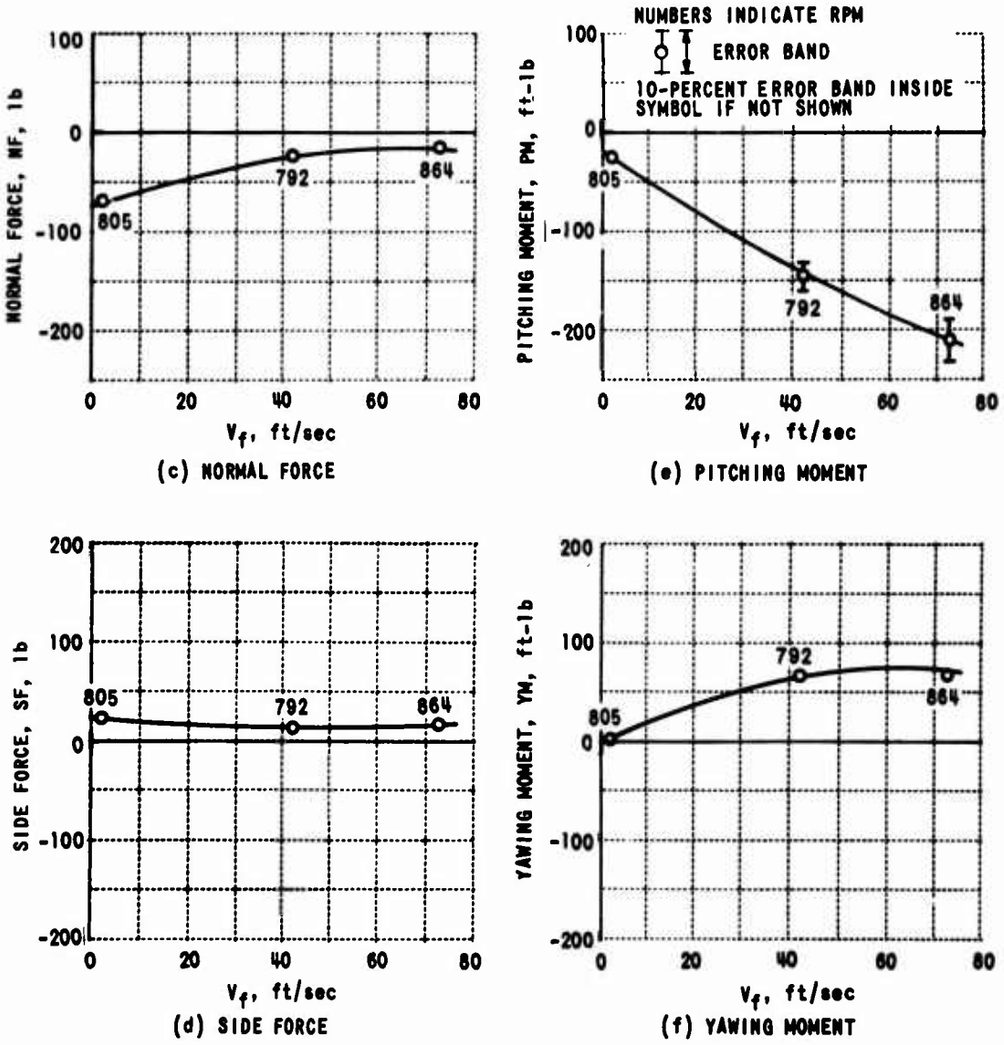

Figure 13. PLOT OF EXPERIMENTAL PERFORMANCE CHARACTERISTICS (T,Q,NF,SF,PM,YM) VS. FREE-STREAM VELOCITY FOR $\tau = 45°$ AND $\beta_R = 10°$. (CONTINUED)

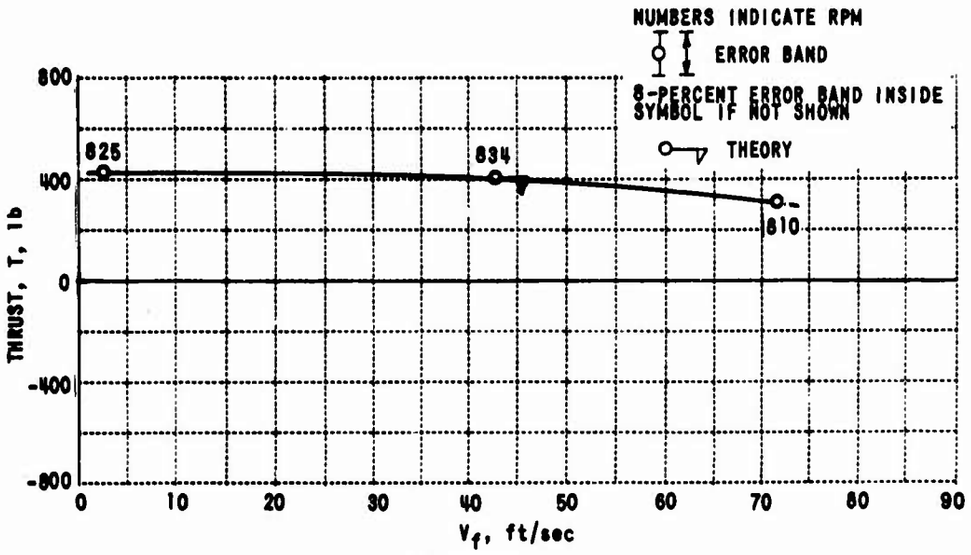

(a) THRUST

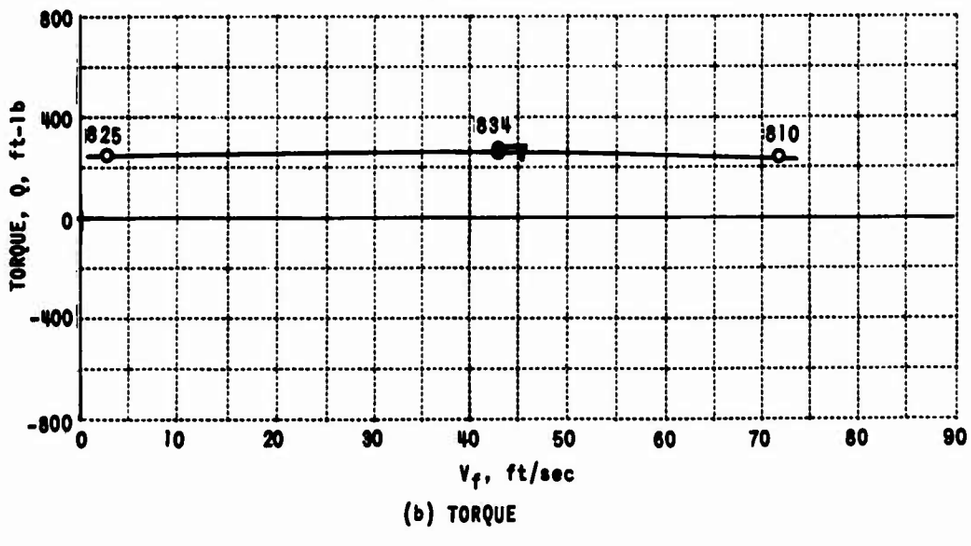

(b) TORQUE

Figure 14. PLOT OF EXPERIMENTAL PERFORMANCE CHARACTERISTICS (T,Q,NF,SF,PM,YM) VS. FREE-STREAM VELOCITY FOR $\tau = 45°$ AND $\beta_R = 15°$.

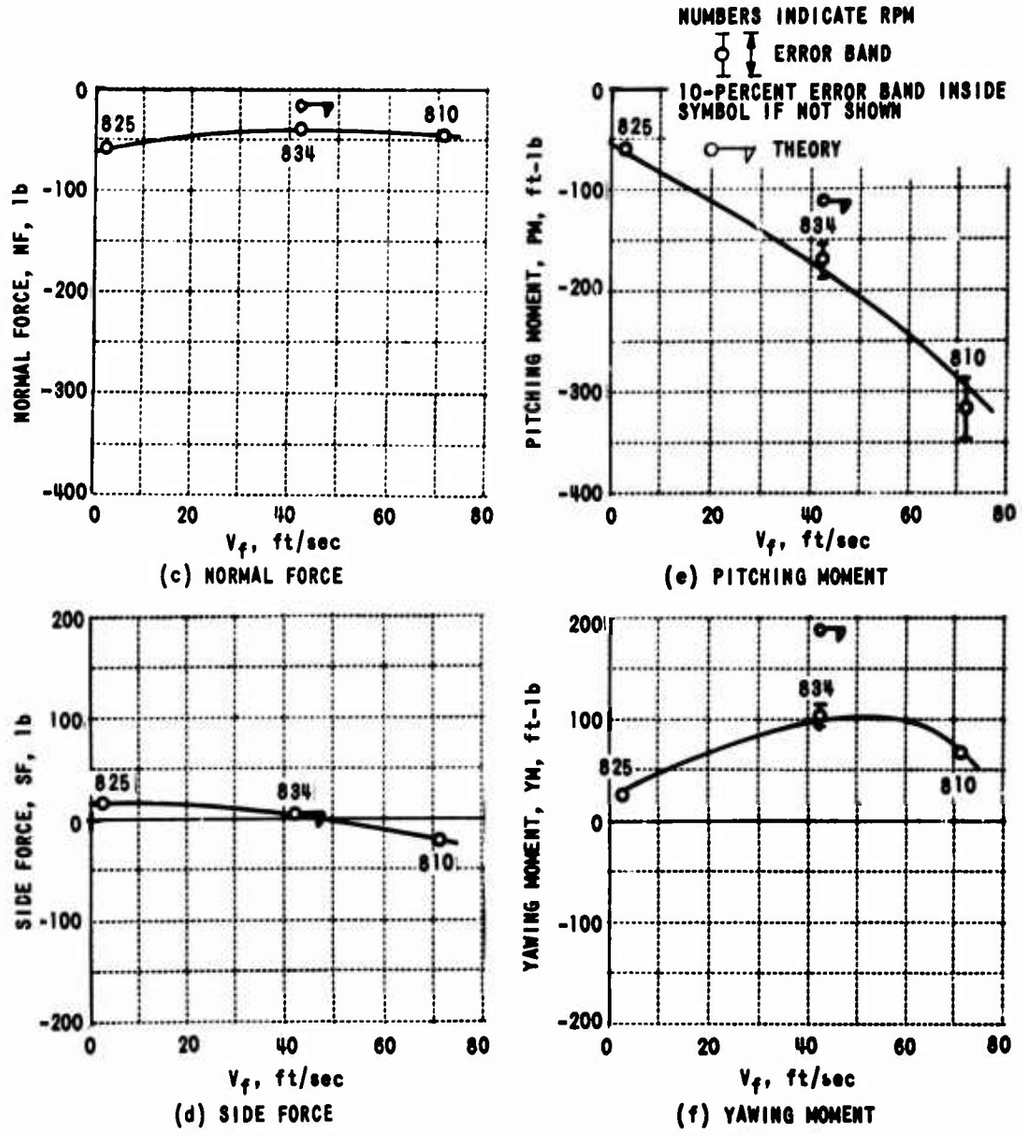

Figure 14. PLOT OF EXPERIMENTAL PERFORMANCE CHARACTERISTICS (T,Q,NF,SF,PM,YM) VS. FREE-STREAM VELOCITY FOR τ = 45° AND β_R = 15°. (CONTINUED)

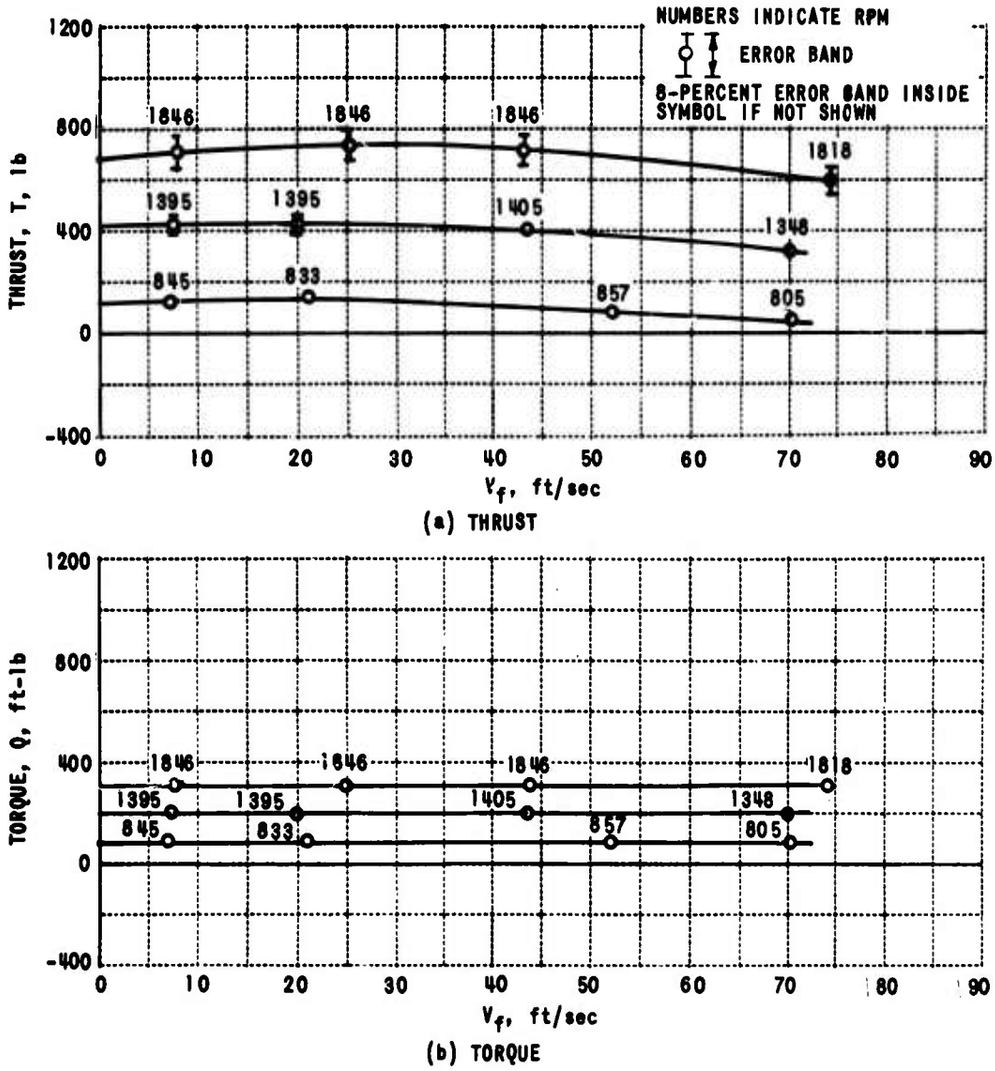

Figure 15. PLOT OF EXPERIMENTAL PERFORMANCE CHARACTERISTICS (T,Q,NF,SF,PM,YM) VS. FREE-STREAM VELOCITY FOR $\tau = 65°$ AND $\beta_R = 5°$.

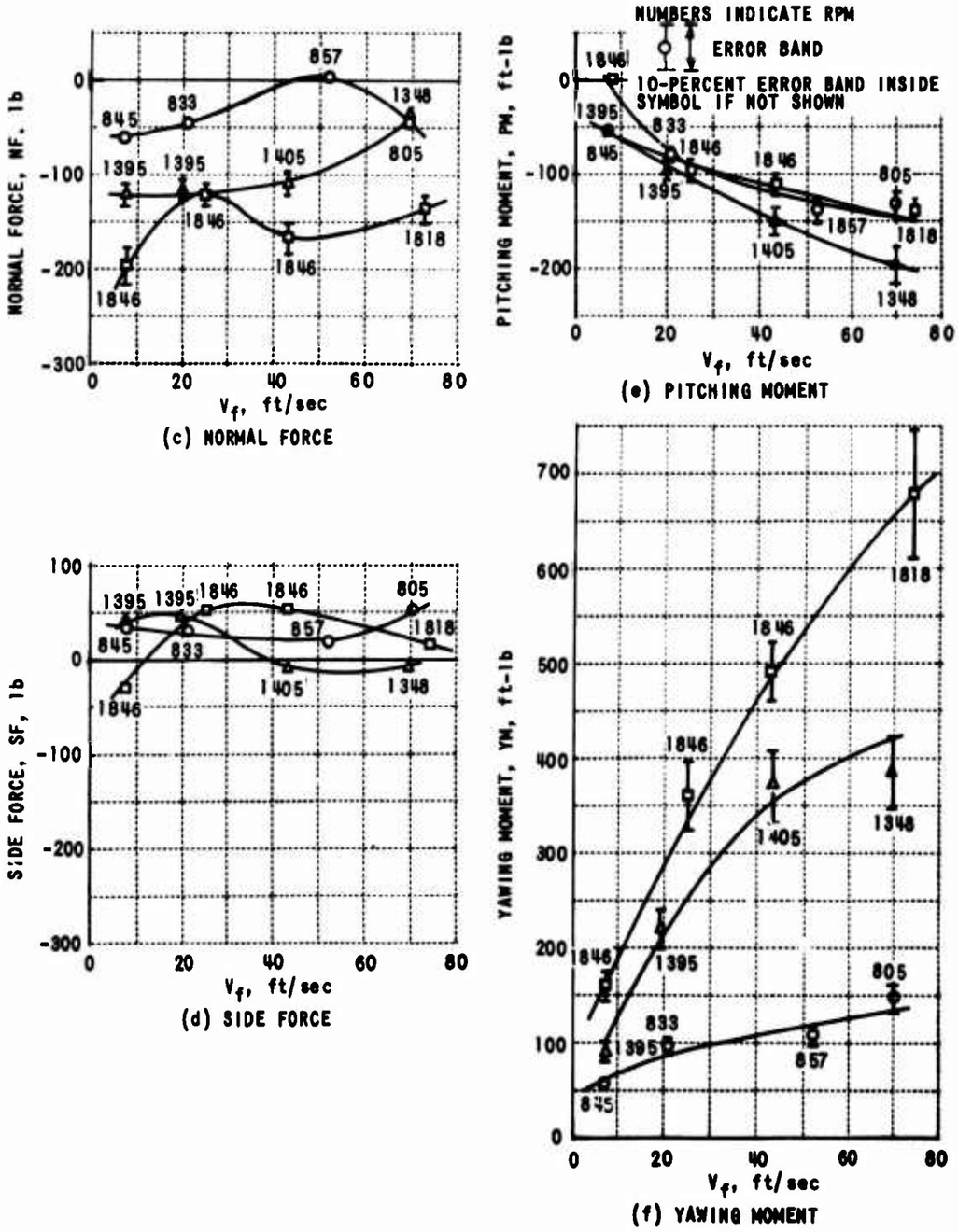

Figure 15. PLOT OF EXPERIMENTAL PERFORMANCE CHARACTERISTICS (T,Q,NF,SF,PM,YM) VS. FREE-STREAM VELOCITY FOR τ = 65° AND β_R = 5°. (CONTINUED)

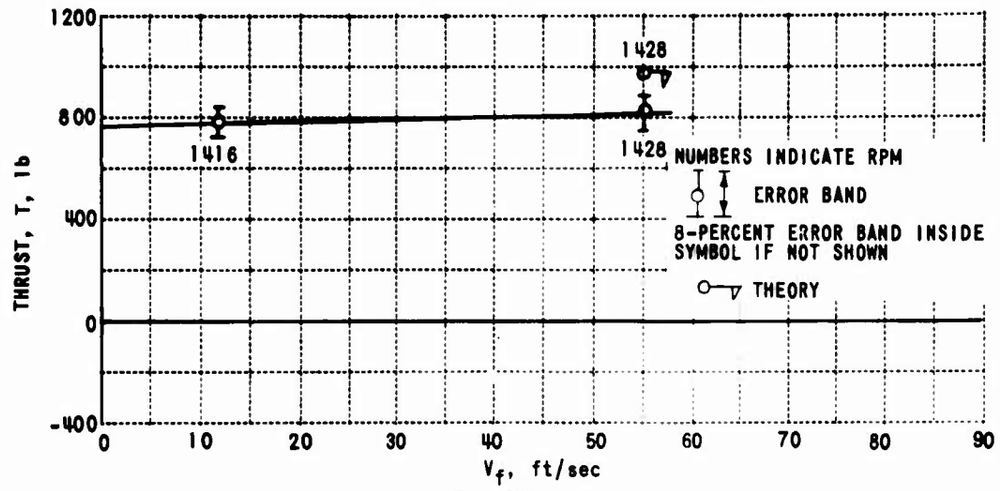

(a) THRUST

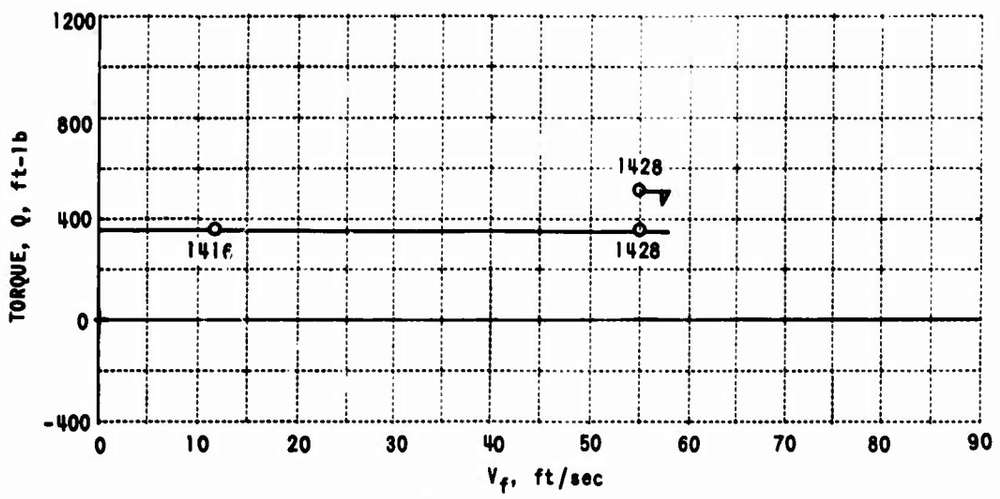

(b) TORQUE

Figure 16. PLOT OF EXPERIMENTAL PERFORMANCE CHARACTERISTICS (T,Q,NF,SF,PM,YM) VS. FREE-STREAM VELOCITY FOR γ = 65° AND β_R = 10°.

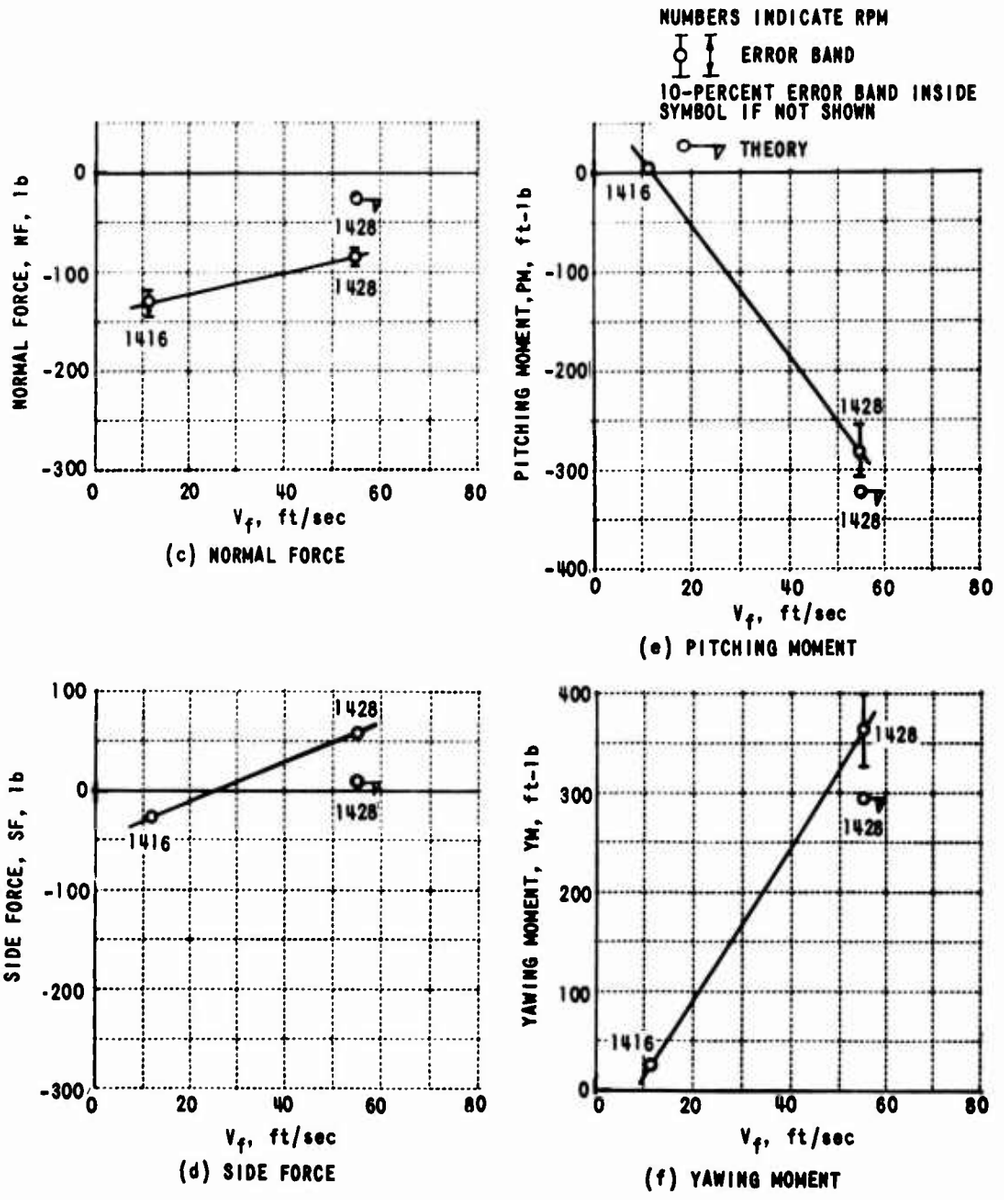

Figure 16. PLOT OF EXPERIMENTAL PERFORMANCE CHARACTERISTICS (T,Q,NF,SF,PM,YM) VS. FREE-STREAM VELOCITY FOR τ = 65° AND β_R = 10°. (CONTINUED)

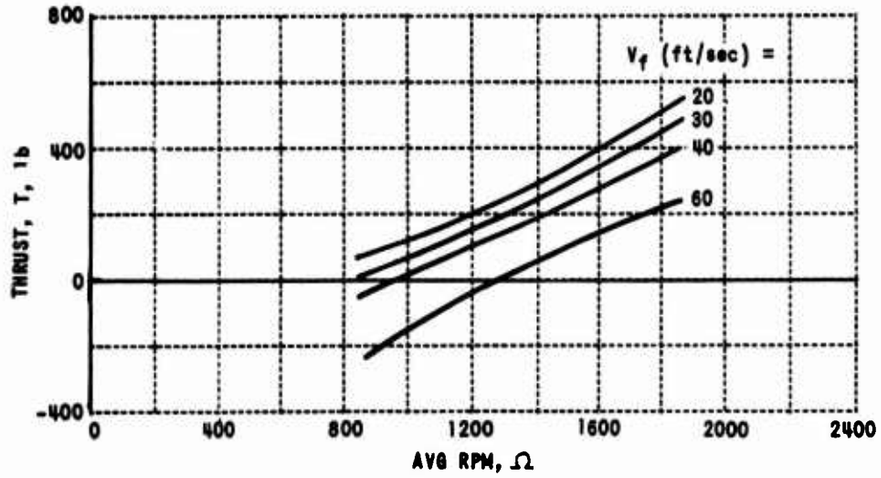

(a) THRUST

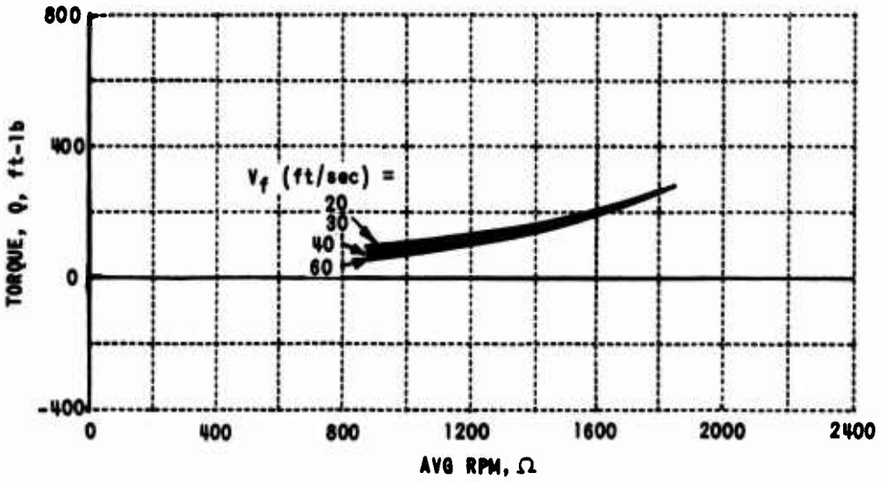

(b) TORQUE

Figure 17. PLOT OF EXPERIMENTAL THRUST AND TORQUE VS. PROPELLER SPEED FOR τ = 0° AND β_R = 5°.

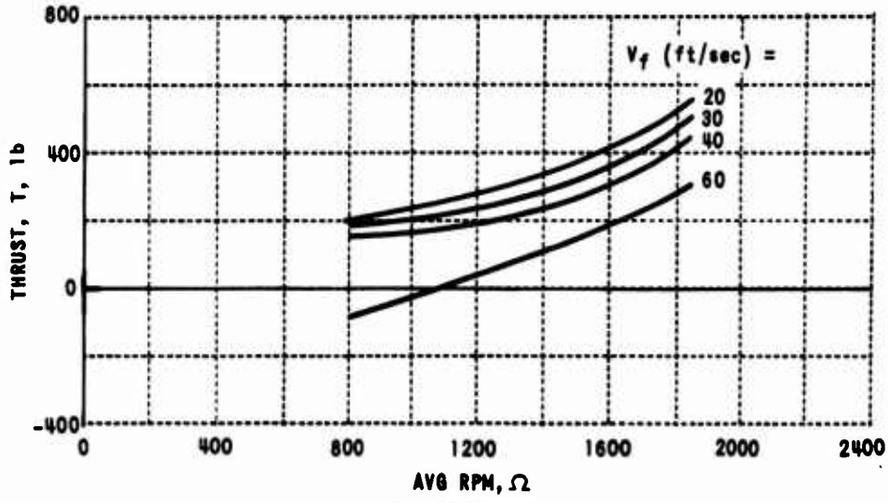

(a) THRUST

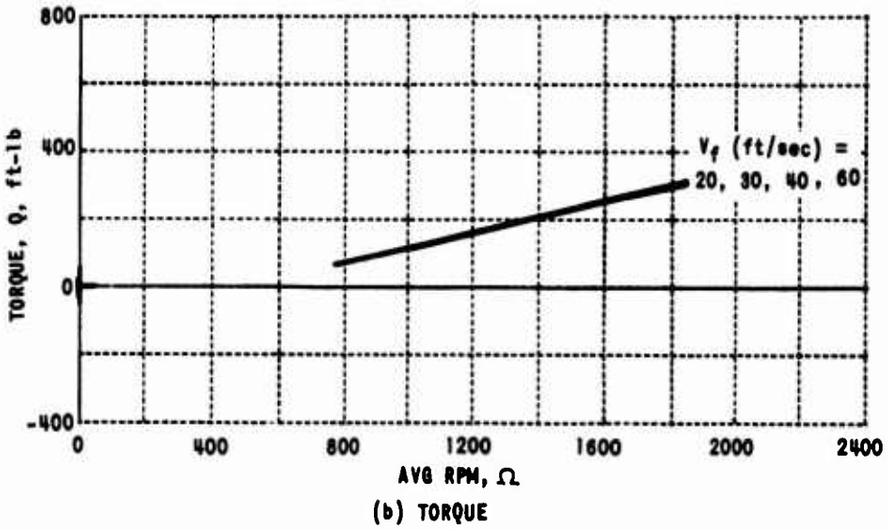

(b) TORQUE

Figure 18. PLOT OF EXPERIMENTAL THRUST AND TORQUE VS. PROPELLER SPEED FOR τ = 30° AND β_R = 5°.

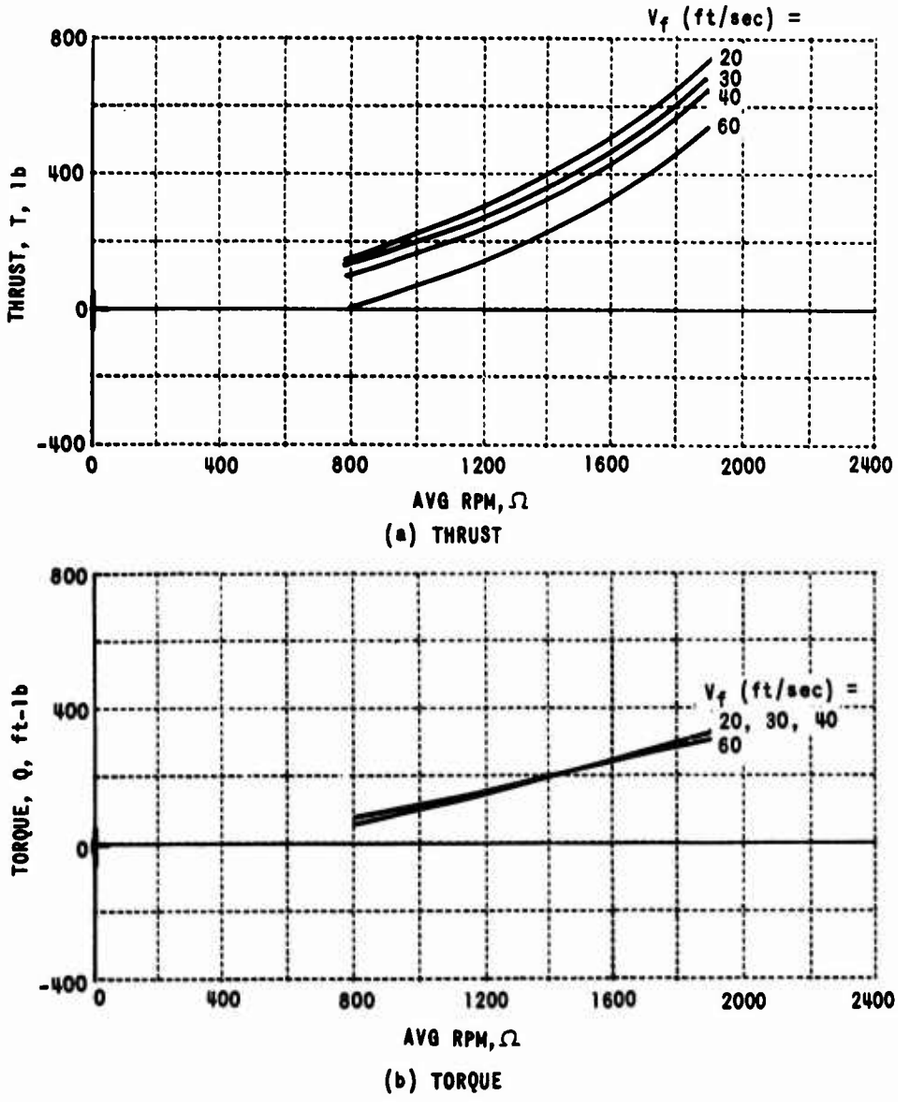

Figure 19. PLOT OF EXPERIMENTAL THRUST AND TORQUE VS. PROPELLER SPEED FOR τ = 45° AND β_R = 5°.

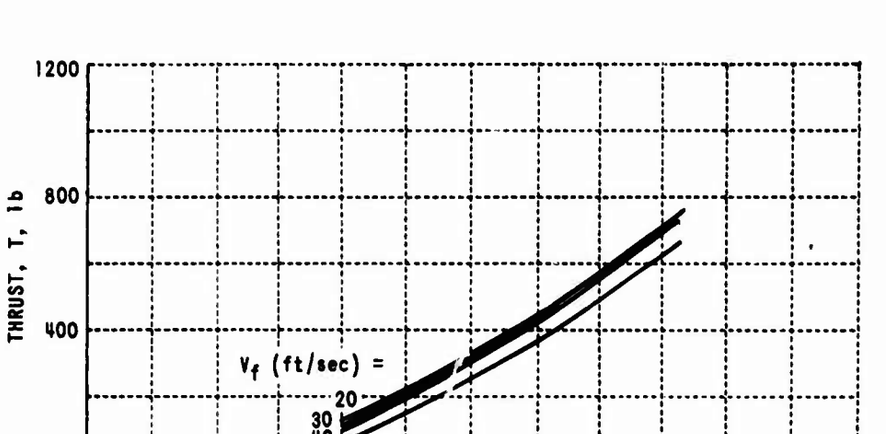

(a) THRUST

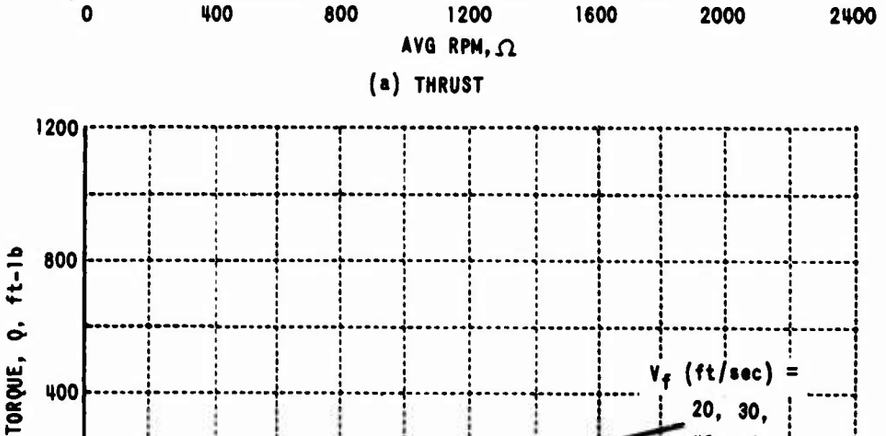

(b) TORQUE

Figure 20. PLOT OF EXPERIMENTAL THRUST AND TORQUE VS. PROPELLER SPEED FOR τ = 65° AND β_R = 5°.

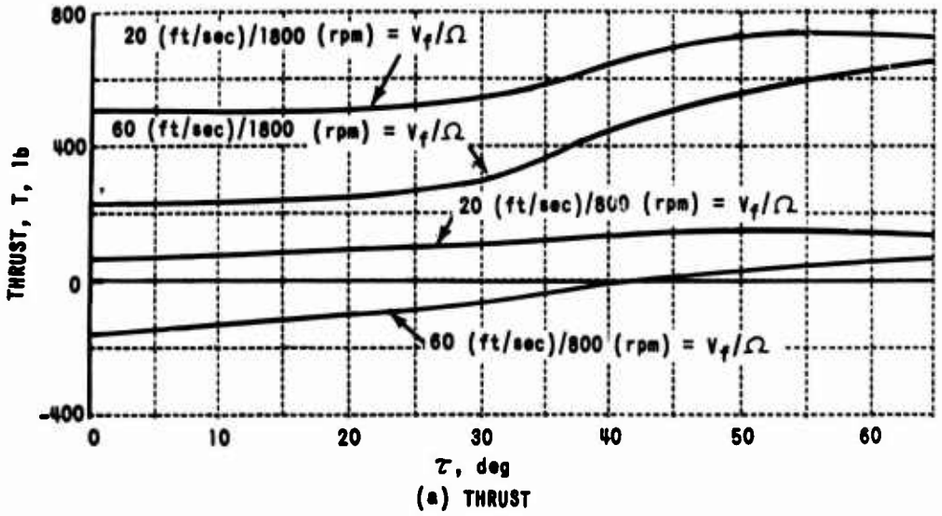

(a) THRUST

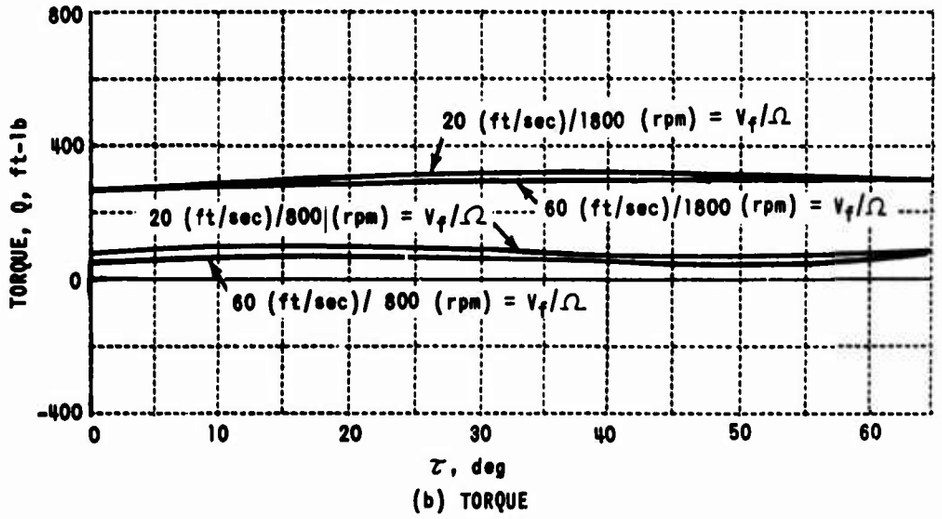

(b) TORQUE

Figure 21. PLOT OF EXPERIMENTAL THRUST AND TORQUE VS. τ FOR $\beta_R = 5°$.

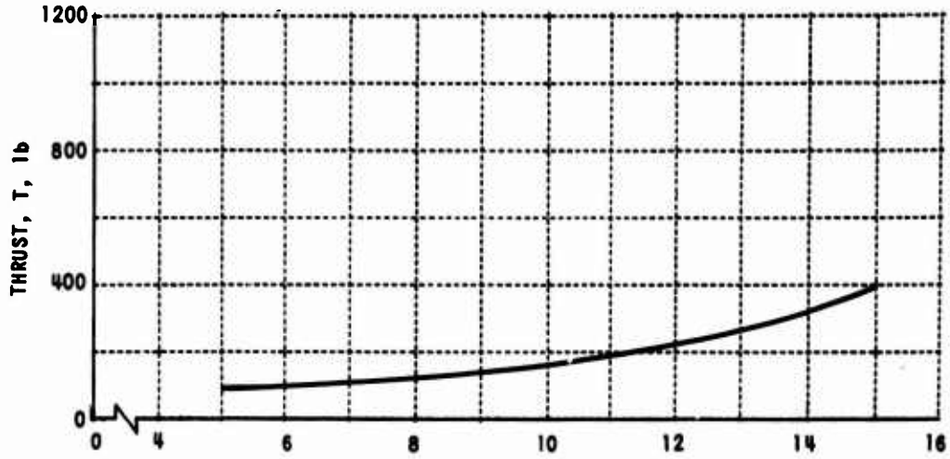

(a) THRUST

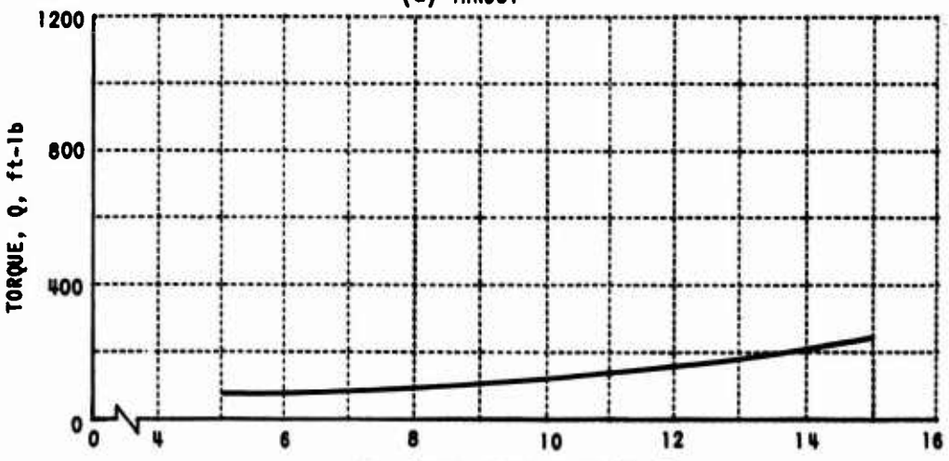

(b) TORQUE

Figure 22. PLOT OF EXPERIMENTAL THRUST AND TORQUE VS. β_R FOR τ = 45°, Ω = 822 R.P.M., AND V_f = 40 FT./SEC.

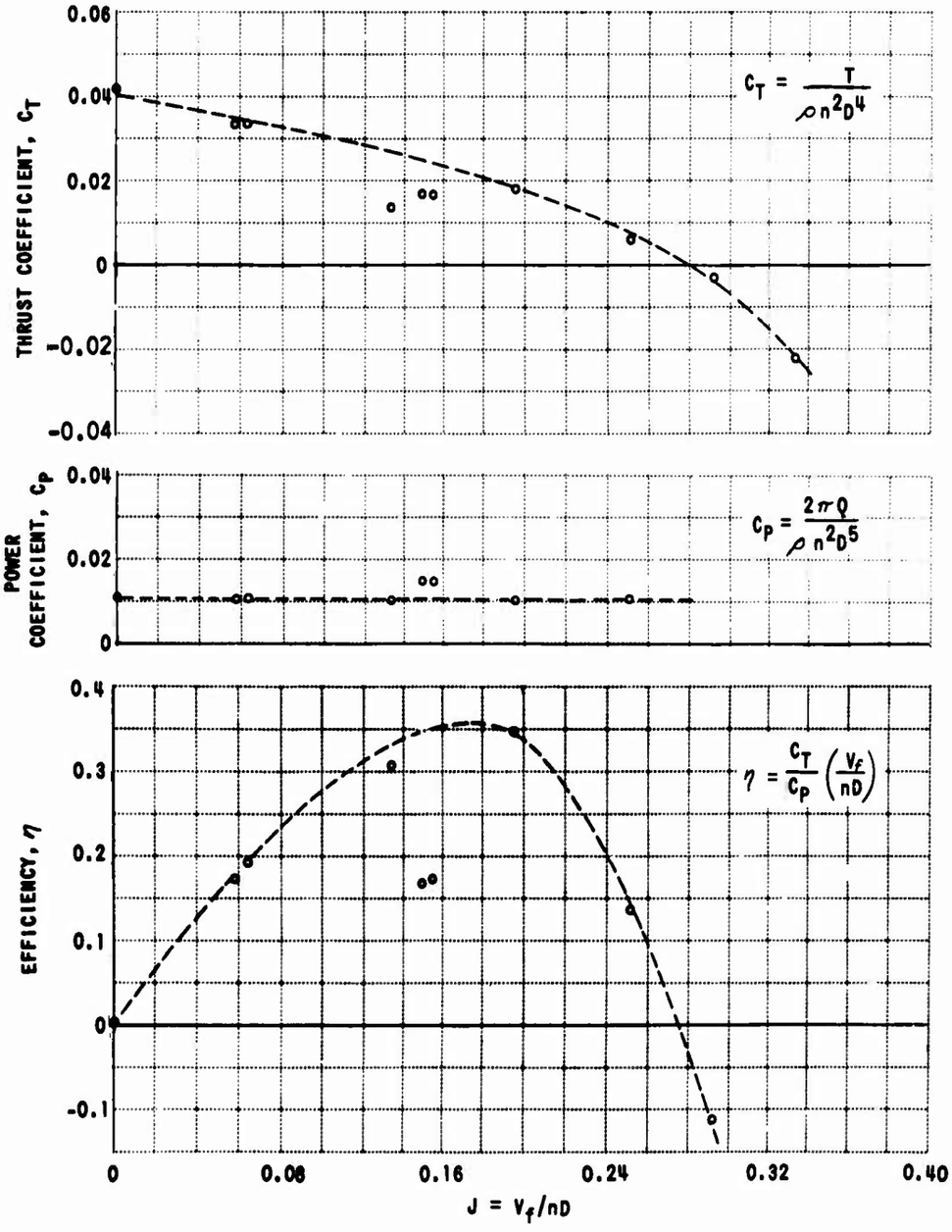

Figure 23. PLOT OF C_T, C_P, AND η VS. J FOR AXIAL FLIGHT AT $\beta_R = 5°$.

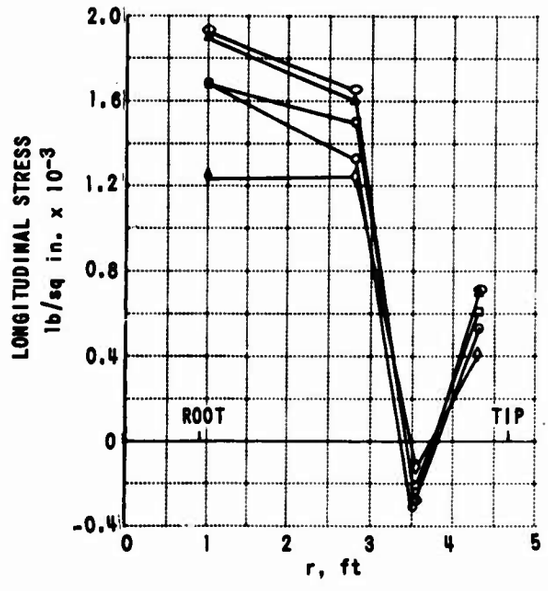

SYMBOL	τ deg	β_R deg	Ω rpm	V_f mph
○	0	5	857	2
△, ⬭	0	5	873	16
□	0	5	822	30
◇	0	5	706	38

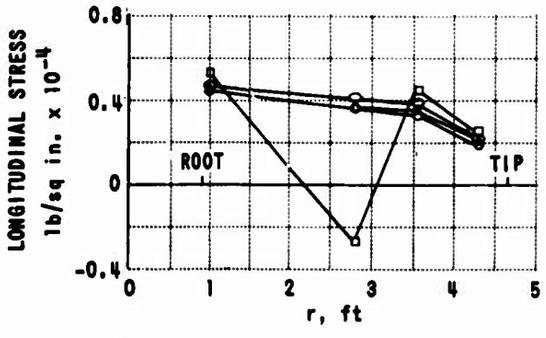

SYMBOL	τ deg	β_R deg	Ω rpm	V_f mph
○	0	5	1395	6
△	0	5	1388	14
⬭	0	5	1395	31
□	0	5	1500	46

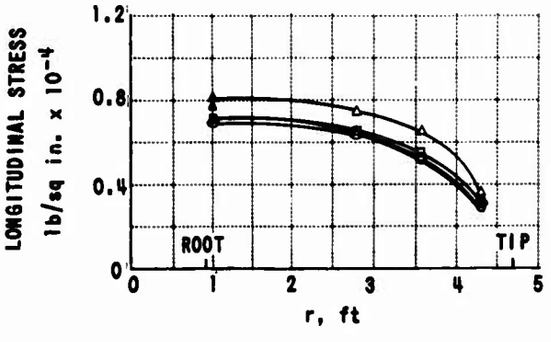

SYMBOL	τ deg	β_R deg	Ω rpm	V_f mph
○	0	5	1818	5
△	0	5	1875	50
⬭	0	5	1818	16
□	0	5	1818	30

Figure 24. SPANWISE DISTRIBUTION OF LONGITUDINAL STRESS AT 50% CHORD FOR τ = 0°, β_R = 5°, AND SEVERAL Ω AND V_f.

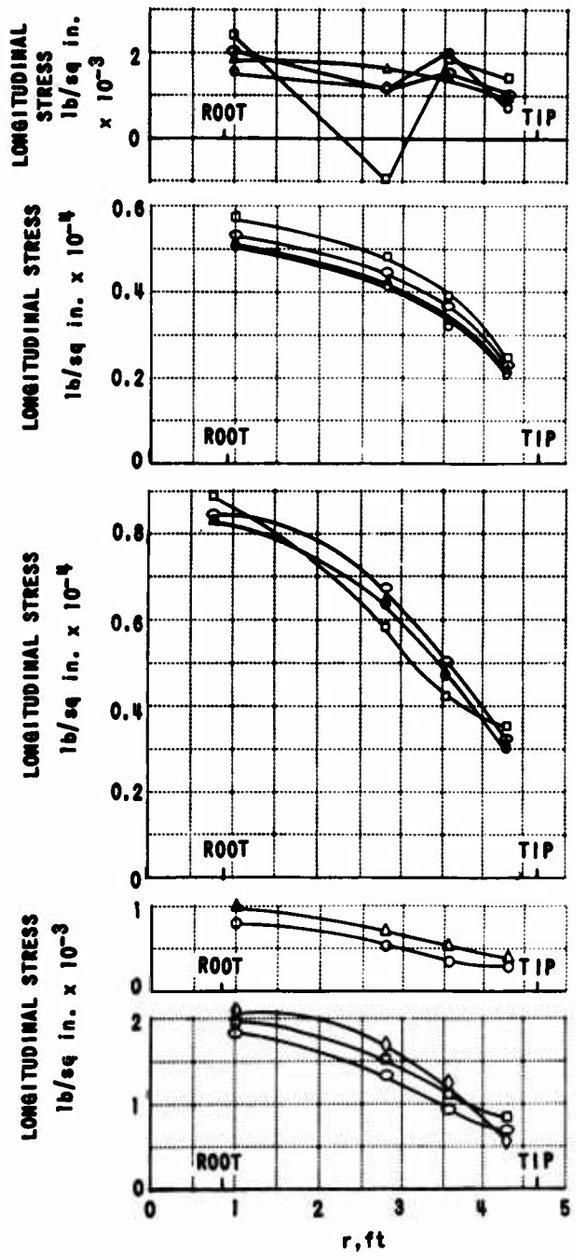

SYMBOL	τ deg	β_R deg	Ω rpm	V_f mph
○	30	5	804	9
△	30	5	857	18
◇	30	5	882	30
□	30	5	882	49

SYMBOL	τ deg	β_R deg	Ω rpm	V_f mph
○	30	5	1363	11
△	30	5	1429	16
◇	30	5	1395	29
□	30	5	1500	45

SYMBOL	τ deg	β_R deg	Ω rpm	V_f mph
○	30	5	1818	8
△	30	5	1818	15
◇	30	5	1818	29
□	30	5	1846	50

SYMBOL	τ deg	β_R deg	Ω rpm	V_f mph
○	30	10	811	12
△	30	10	874	33

SYMBOL	τ deg	β_R deg	Ω rpm	V_f mph
◇	30	10	1255	11
□	30	10	1277	32
◊	30	10	1277	48

Figure 25. SPANWISE DISTRIBUTION OF LONGITUDINAL STRESS AT 50% CHORD FOR τ = 30°, β_R = 5° AND 10°, AND SEVERAL Ω AND V_f.

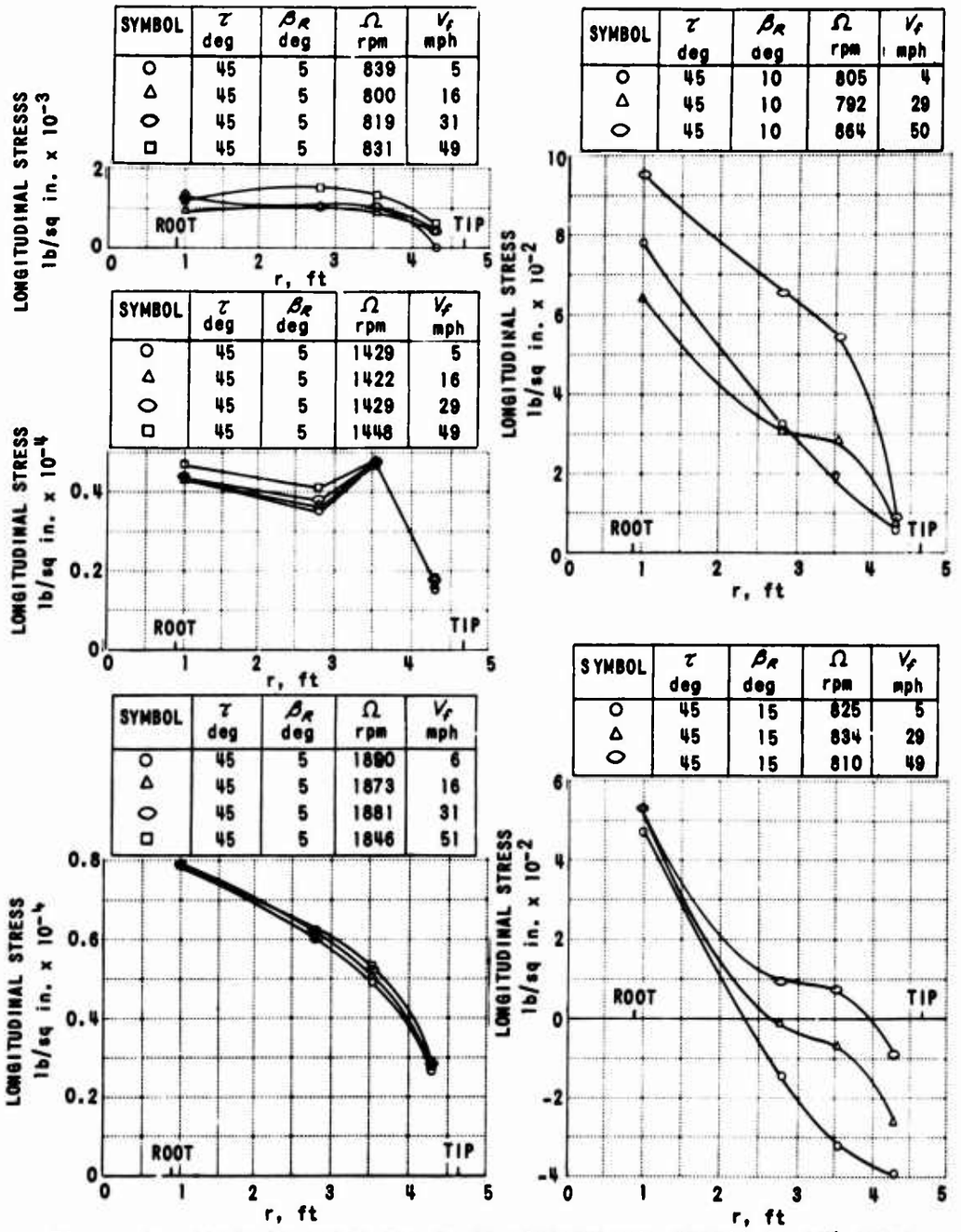

Figure 26. SPANWISE DISTRIBUTION OF LONGITUDINAL STRESS AT 50% CHORD FOR τ = 45°, β_R = 5°, 10°, AND 15°, AND SEVERAL Ω AND V_f.

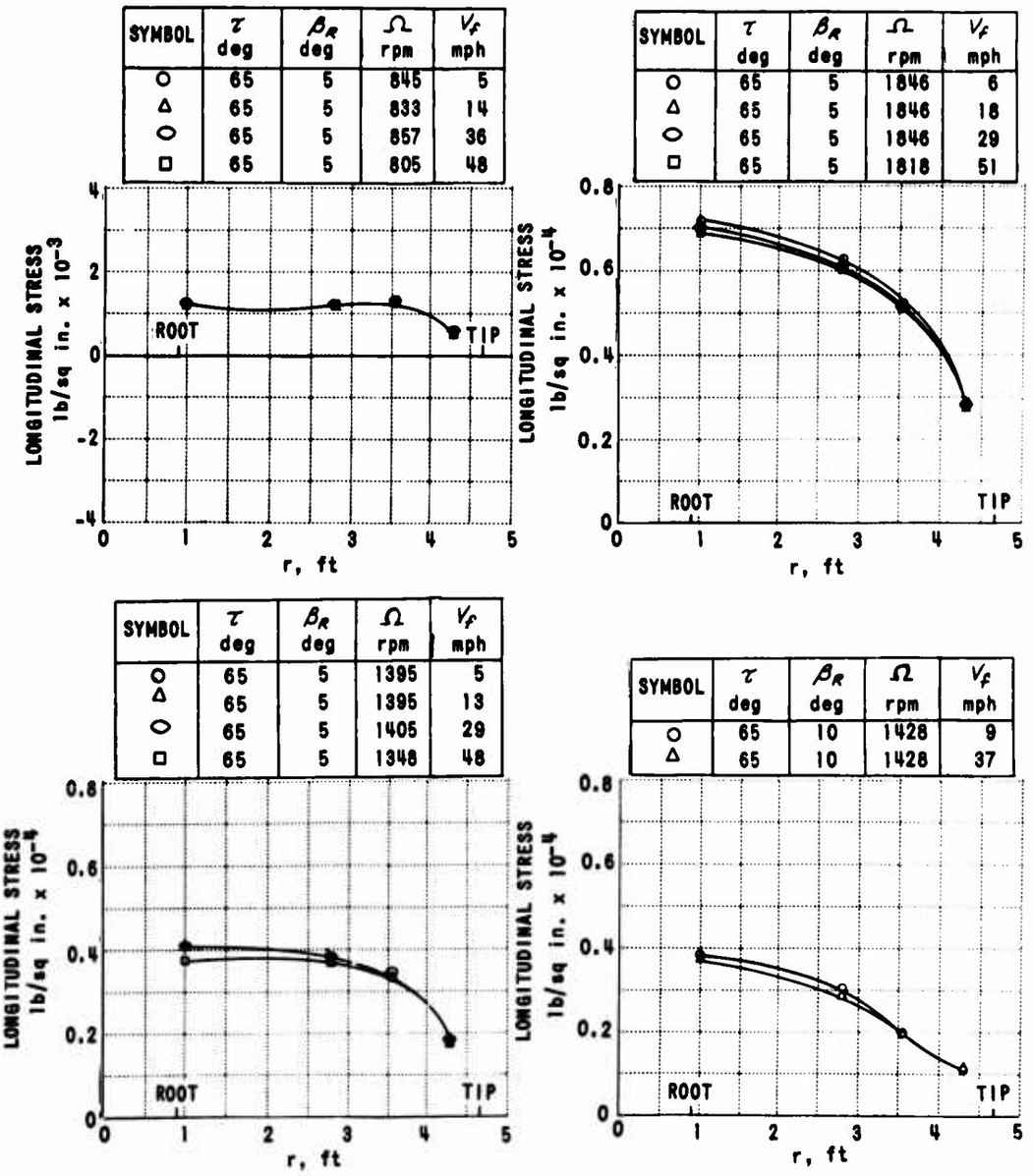

Figure 27. SPANWISE DISTRIBUTION OF LONGITUDINAL STRESS AT 50% CHORD FOR τ = 65°, β_R = 5° AND 10°, AND SEVERAL Ω AND V_f.

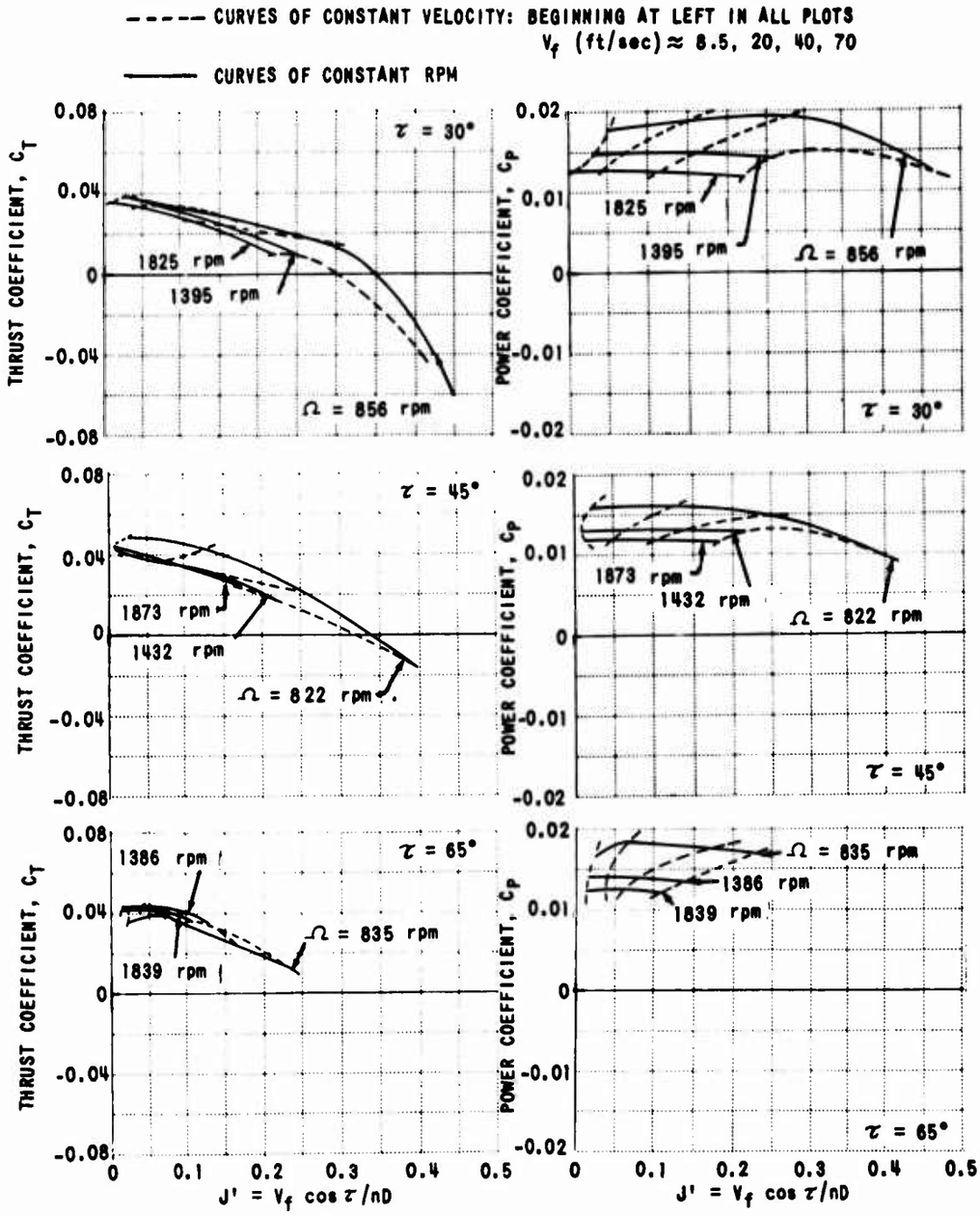

Figure 28. PLOT OF C_T AND C_p VS. J' AT β_R = 5° FOR VARIOUS τ AND Ω.

REFERENCES

1. Trenka, A. R., DEVELOPMENT OF A METHOD FOR PREDICTING THE PERFORMANCE AND STRESSES OF VTOL-TYPE PROPELLERS, Cornell Aeronautical Laboratory, Inc., USAAVLABS Technical Report 66-26, U. S. Army Aviation Materiel Laboratories, Fort Eustis, Virginia, June 1966.

2. Erickson, J. C., Jr., Ladden, R. M., Borst, H. V., and Ordway, D. E., A THEORY FOR VTOL PROPELLER OPERATION IN A STATIC CONDITION, USAAVLABS Technical Report 65-69, U. S. Army Aviation Materiel Laboratories, Fort Eustis, Virginia, October 1965.

3. Sullivan, E. M., A TEST APPARATUS FOR SMALL ROTOR-CRAFT, Vol. I, CAL Report No. SG-1195-S-3, Cornell Aeronautical Laboratory, Inc., Buffalo, New York, November 1959.

4. Heyson, H. H. and Katzoff, S., INDUCED VELOCITIES NEAR A LIFTING ROTOR WITH NONUNIFORM DISK LOADING, NACA Report No. 1319, 1957.

5. Yaggy, P. F., and Rogallo, V. L., A WIND-TUNNEL INVESTIGATION OF THREE PROPELLERS THROUGH AN ANGLE-OF-ATTACK RANGE FROM 0^{o} TO 85^{o}, NASA Technical Note D-318, May 1960.

APPENDIX I

DERIVATION OF THE INPLANE FORCE AND MOMENT FROM DATA OBTAINED ON THE ROTATING BALANCE

The rotating balance designed and built by NASA has the characteristic that it responds only to a component of inplane force and moment. For example, consider a rectangular beam cantilevered at one end (see sketch).

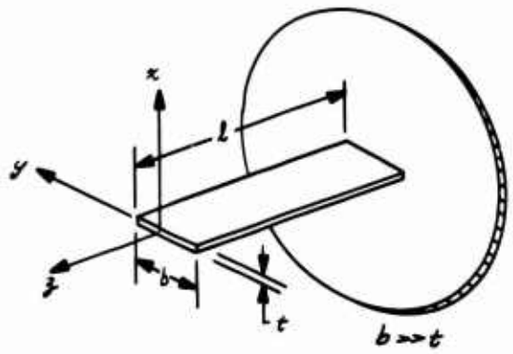

The beam would deflect most due to a load applied along the x axis. Hence, the x axis would be referred to as the sensitive axis. In the analogous situation in the balance, this axis is fixed in the balance and rotates with it. The balance is instrumented to respond only to loads along this axis. Thus, at any instant of time, the balance will put out a signal which is proportional to the component of the inplane force (or moment) along the sensitive axis. Consider Figure 29 where X_o, Y_o, Z_o is a coordinate system fixed in the prop plane such that the Z_o axis lies along the axis of rotation. Then, the normal force component (NF) and the yawing moment component (YM) are defined to be components of the inplane force and moment in the X_o direction, and the side force (SF) and pitching moment (PM) are defined as the components in the Y_o direction.

The angular orientation of the sensitive axis is defined by $\varphi = \alpha$ measured from the X_o axis.

Let $\vec{R}$ be the vector representation of the total inplane force (moment) when $\psi = \alpha$,

$\vec{i}, \vec{j}, \vec{v}$ be the unit vectors along X_o, Y_o, and "sensitive" axes, respectively.

α be the angle between the sensitive axis and the X_o axis,

ψ_R be the angle between $\vec{R}$ and X_o.

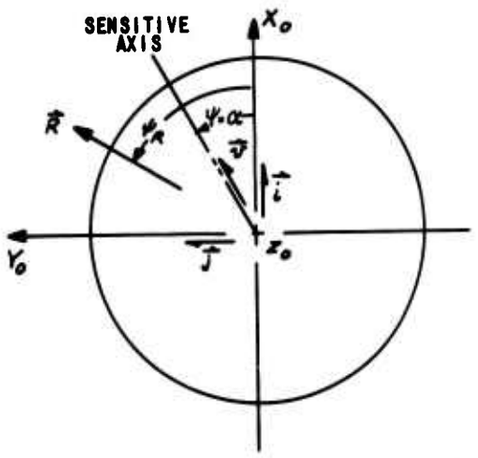

Figure 29. SCHEMATIC OF RESULTANT INPLANE FORCE.

The component of $\vec{R}$ along the sensitive axis is given as

$$B = \vec{R} \cdot \vec{v}. \tag{9}$$

But, for the inplane force, say,

$$\vec{R} = NF\vec{i} + SF\vec{j} \tag{10}$$

and

$$\vec{v} = (\cos \alpha)\vec{i} + (\sin \alpha)\vec{j}. \tag{11}$$

Thus,

$$B = NF \cos \alpha + SF \sin \alpha. \tag{12}$$

For a three-bladed isolated propeller in steady flight, the loads repeat three times per prop revolution. Hence, every 120 degrees, $\vec{R}$ has the same magnitude and orientation as shown in Figure 29, but the angular position of the sensitive axis has shifted by 120 degrees. The equations describing this condition are

$$B_1 = NF \cos \alpha + SF \sin \alpha \qquad (13)$$

$$B_2 = -NF \sin (30 + \alpha) + SF \cos (30 + \alpha) \qquad (14)$$

where

B_1 = the balance reading at $\psi = \alpha$

B_2 = the balance reading at $\psi = \alpha + 120$.

From the set of Equations (13) and (14), the unknowns NF and SF may be solved to obtain

$$NF = \frac{2}{\sqrt{3}} \left[B_1 \cos (30 + \alpha) - B_2 \sin \alpha \right] \qquad (15)$$

$$SF = \frac{2}{\sqrt{3}} \left[B_2 \cos \alpha + B_1 \sin (30 + \alpha) \right]. \qquad (16)$$

These values of NF and SF exist every 120 degrees.

For the balance system in hand, the quantities B_1 and B_2 represent the output signal denoted $\overline{NF}$ at two azimuthal positions, α and $\alpha + 120$ degrees. Thus, by knowing the angular position of the sensitive axis with respect to the X_0 axis, the $\overline{NF}$ signal may be sampled in such a fashion as to yield the azimuthal history of NF and SF.

The same comments apply for the pitching and yawing moments.

APPENDIX II

LISTING OF THE DATA REDUCTION PROGRAM

INPUTS REQUIRED

Card 1	*ICHK*	0 - Does not print uncorrected performance results 1 - Prints uncorrected results
Card 2	*EYM*	Young's modulus (p. s. i.)
	PR	Poisson's ratio
	PSIB	Angular position of balance sensitive axis with respect to reference blade (degrees)
	DELPSI	Azimuthal increment at which data is sampled (degrees)
Card 3	*RM(I), I = 1,4*	Radian position from prop center of rotation to each strain-gage location (feet)
Cards 4 to 7	*PCC(I, J), J = 1,4; I = 1,4*	Elements of performance calibration matrix (load per inch oscillograph deflection)

Card 8		Distance from reference line of record to no-load trace for each performance quantity (inches)
Cards 9 to 12	$SCC(I,J)$, $I = 1,3$; $J = 1,4$	Elements of strain calibration matrix (10^{-6} inches per inch per inch oscillograph deflection)
Cards 13 to 16	$SZD(J,K)$, $K = 1,3$; $J = 1,4$	Distance from reference line on record to no-load trace for each strain quantity (inches)

Performance Case

Card 17	Case $ID(I)$, $I = 1,8$	Identification of cases to be analyzed
	Type	P - Indicates performance data follows
	$NPTS$	S - Indicates strain data follows
	$SCTF$	Number of increments at which data is read
		F - Plot unscaled data
		T - Plot scaled data
	$YMIN$	Minimum Y value to be plotted
	DY	Scale of Y axis per inch

*Card 18	$PA(I),\ I = 1,4$	Attenuation ratio for performance
Card 18	$SA(I,J),\ I = 1,3;$ $J = 1,4$	Attenuation ratio for strains
Cards 19 to 22	$PD(I,J),\ I = 1,NPTS;$ $J = 1,4$	Performance deflections from reference trace (inches)
Cards 19 to 30	$SD(I,J,K),\ I = 1,NPTS;$ $K = 1,3;\ J = 1,4$	Strain deflections from reference trace (inches)

* In performance, first case should be gravity tare corrections.

```
$IBFTC SSVTOL  LIST,DECK,REF
       DIMENSION SCC(3,4),PCC(4,4),CASEID( 8),PA(4),PD(30,4),T(30),Q(30),
      1EMB(30,2),PSIR(30),NF(30),SF(30),PM(30),YM(30),SA(3,4),SD(30,4,3),
      2E(3),TS(30,4),SS(30,4)
       DIMENSION PZD(4),SZD(4,3),ASIGN(4,3),TG(15),QG(15),NFG(15),
      1SFG(15),YMG(15),PMG(15),RM(4)
       DIMENSION PERF(4),STRSS(4)
       REAL NF,NFG
       LOGICAL SCTF
       DATA ASIGN/-1.0,1.0,1.0,1.0,1.0,-1.0,1.0,-1.0,+1.0,1.0,1.0,-1.0/
       DATA P/1HP/,NCASE/0/
       DATA PERF/24HT      Q      NF     PM     /
       DATA STRSS/24HR1     R2     R3     R4     /
       CALL DVDCHK(1)
       READ (5,1) ICHK
     1 FORMAT (6I12)
       READ (5,2) EYM,PR,PSIB,DELPSI
     2 FORMAT (4E12.5)
       READ (5,2) (RM(I),I=1,4)
       READ (5,2) ((PCC(I,J),J=1,4),I=1,4)
       READ (5,2) (PZD(I),I=1,4)
       READ (5,50) ((SCC(I,J),I=1,3),J=1,4)
    50 FORMAT (3E12.5)
       READ (5,50) ((SZD(J,K),K=1,3),J=1,4)
       WRITE (6,3)
     3 FORMAT (50H1EXPERIMENTAL DATA REDUCTION PROGRAM - A.TRENKA/SS/)
       WRITE (6,90) ICHK
    90 FORMAT (6HOICHK=,I2)
       WRITE (6,14) EYM,PR,PSIB,DELPSI
    14 FORMAT    (5HOEYM=,E12.5,2X,3HPR=,E12.5,2X,5HPSIB=,E12.5,2X,
      17HDELPSI=,E12.5)
       WRITE (6,55) (RM(I),I=1,4)
    55 FORMAT (3HORM/1X,4E15.5)
       WRITE (6,5) ((PCC(I,J),J=1,4),I=1,4)
     5 FORMAT (4HOPCC/(1X,4E15.5))
       WRITE (6,51) (PZD(I),I=1,4)
    51 FORMAT (16HOPZD (T,Q,NF,PM)/1X,4F7.2)
       WRITE (6,4)
     4 FORMAT (4HOSCC)
       DO 92 J=1,4
       WRITE (6,93) STRSS(J),(SCC(I,J),I=1,3)
    93 FORMAT (1X,A2/1X,3E15.5)
    92 CONTINUE
       WRITE (6,52) ((SZD(J,K),K=1,3),J=1,4)
    52 FORMAT (18HOSZD (R1,R2,R3,R4)/1X,4(3F6.2,3X))
       YMF=EYM/(1.0-PR**2)
       RPD=0.017453292
       PSIBR=PSIB*RPD
       DELPSR=DELPSI*RPD
       KPTS=360.0/DELPSI
       DO 40 I=1,KPTS
       PSIR(I)=FLOAT(I-1)*DELPSR
       TG(I)=0.0
       QG(I)=0.0
```

```
      NFG(I)=0.0
      SFG(I)=0.0
      PMG(I)=0.0
      YMG(I)=0.0
   40 CONTINUE
 1000 READ (5,6) (CASEID(I),I=1,8), TYPE,NPTS,SCTF,YMIN,DY
    6 FORMAT  (8A6,A1,I3,L4,2E12.5)
      WRITE (6,7) (CASEID(I),I=1,8), TYPE,NPTS,SCTF,YMIN,DY
    7 FORMAT (1H1, 8A6/1X,5HTYPE=,A1,2X,5HNPTS=I3,2X,5HSCTF=,L2,2X,
     15HYMIN=,E12.5,2X,3HDY=,E12.5)
      IF (TYPE.EQ.P) GO TO 100
      GO TO 200
  100 READ (5,2) (PA(I),I=1,4)
      WRITE (6,8) (PA(I),I=1,4)
    8 FORMAT (3HOPA/1X,4E15.5)
      WRITE (6,9)
    9 FORMAT (3HOPD)
      DO 60  J=1,4
      READ (5,27) (PD(I,J),I=1,NPTS)
   27 FORMAT (15F4.2)
      WRITE (6,61) PERF(J),(PD(I,J),I=1,NPTS)
   61 FORMAT (1X,A2/(1X,15F7.2))
   60 CONTINUE
   12 DO 15  I=1,NPTS
      T(I) = 0.0
      Q(I) = 0.0
      DO 11  J=1,4
      PAPD = PA(J)*(PZD(J)-PD(I,J))
      T(I) = T(I)+PCC(1,J)*PAPD
      Q(I) = Q(I)+PCC(2,J)*PAPD
   11 CONTINUE
      DO 16  L=1,2
      FMB(I,L)=0.0
      DO 17  J=1,4
      PAPD = PA(J)*(PZD(J)-PD(I,J))
      FMB(I,L)=FMB(I,L)+PCC(L+2,J)*PAPD
   17 CONTINUE
   16 CONTINUE
   15 CONTINUE
      IF (ICHK.EQ.0) GO TO 80
      WRITE (6,81)
   81 FORMAT (24H1UNCORRECTED PERFORMANCE)
      WRITE (6,25)
   80 DO 20  I=1,NPTS
      ALPHA1=PSIR(I)-PSIBR
      SINA1=SIN(ALPHA1)
      COSA1=COS(ALPHA1)
      SINA2=(0.8660254*SINA1+0.5*COSA1)
      COSA2=(0.8660254*COSA1-0.5*SINA1)
      IT2=MOD(I+4,NPTS)+1
      DO 21  L=1,2
      BT1=FMB(I,L)
      BT2=FMB(IT2,L)
      GO TO (23,24),L
   23 NF(I)=1.1547*(BT1*COSA2-BT2*SINA1)
```

```
      SF(I)=1.1547*(BT2*COSA1+BT1*SINA2)
      GO TO 21
   24 PM(I)=1.1547*(BT2*COSA1+BT1*SINA2)
      YM(I)=1.1547*(BT1*COSA2-BT2*SINA1)
      IF (ICHK.EQ.1) WRITE (6,26) (I,T(I),Q(I),NF(I),SF(I),PM(I),YM(I))
   21 CONTINUE
      T(I)=T(I)-TG(I)
      Q(I)=Q(I)-QG(I)
      NF(I)=NF(I)-NFG(I)
      SF(I)=SF(I)-SFG(I)
      PM(I)=PM(I)-PMG(I)
      YM(I)=YM(I)-YMG(I)
   20 CONTINUE
      IF (NCASE.NE.0) GO TO 53
      DO 54  I=1,NPTS
      TG(I)=T(I)
      QG(I)=Q(I)
      NFG(I)=NF(I)
      SFG(I)=SF(I)
      PMG(I)=PM(I)
      YMG(I)=YM(I)
   54 CONTINUE
      NCASE = 1
   53 WRITE (6,82)
   82 FORMAT (27H1TARE CORRECTED PERFORMANCE)
      WRITE (6,25)
   25 FORMAT (1H0,2X,1HI,6X,5HT(LB),10X,8HQ(FT-LB),7X,6HNF(LB),9X,
     16HSF(LB),9X,9HPM(FT-LB),6X,9HYM(FT-LB))
      WRITE (6,26) (I,T(I),Q(I),NF(I),SF(I),PM(I),YM(I),I=1,NPTS)
   26 FORMAT (I4,6E15.5/)
      CALL HARMON (T,18HPROP THRUST  LB   ,18,0,NPTS,0.0)
      CALL HARMON (Q,18HPROP TORQUE  FT-LB,18,0,NPTS,0.0)
      CALL HARMON (NF,24HPROP NORMAL FORCE  LB   ,24,0,NPTS,0.0)
      CALL HARMON (SF,24HPROP SIDE FORCE  LB     ,24,0,NPTS,0.0)
      CALL HARMON (PM,30HPROP PITCHING MOMENT  FT-LB   ,30,0,NPTS,0.0)
      CALL HARMON (YM,30HPROP YAWING MOMENT  FT-LB     ,30,0,NPTS,0.0)
      GO TO 1000
  200 READ (5,98) ((SA(I,J),I=1,3),J=1,4)
   98 FORMAT (12F6.0)
      WRITE (6,99) ((SA(I,J),I=1,3),J=1,4)
   99 FORMAT (17HOSA (R1,R2,R3,R4)/1X,4(3F6.2,3X))
      WRITE (6,29)
   29 FORMAT (3HOSD)
      DO 70  J=1,4
      DO 71  K=1,3
      READ (5,27) (SD(I,J,K),I=1,NPTS)
   71 CONTINUE
      WRITE (6,61) STRSS(J),((SD(I,J,K),I=1,NPTS),K=1,3)
   70 CONTINUE
      DO 30  J=1,4
      WRITE (6,33) STRSS(J)
   33 FORMAT (1H1,A2/1X,1HI,8X,2HE1,11X,2HE2,11X,2HE3,11X,2HEZ,11X,2HEX,
     16X,6HTHETAD,5X,4HSIGZ,9X,4HSIGX,5X,12HTS(LB/SQ IN),1X,
     212HSS(LB/SQ IN))
```

```
      DO 31  I=1,NPTS
      DO 32  K=1,3
      E(K)=SCC(K,J)*SA(K,J)*(SD(I,J,K)-SZD(J,K))*ASIGN(I,K)
   32 CONTINUE
      A=(E(1)+E(3))*0.5
      B=((E(1)-E(2))**2+(E(3)-E(2))**2)*0.5
      C=SQRT(B)
      EZ=A+C
      EX=A-C
      ATN=2.0*(A-E(2))
      ATD=E(3)-E(1)
      THETA=ATAN2(ATN,ATD)
      THETAD=THETA*57.2957795
      SIGZ=YMF*(EZ+PR*EX)
      SIGX=YMF*(EX+PR*EZ)
      SIGZPX=SIGZ+SIGX
      SIGZMX=SIGZ-SIGX
      TS(I,J)=(SIGZPX-SIGZMX*SIN(THETA))*0.5
      SS(I,J)=- SIGZMX*COS(THETA)*0.5
      WRITE (6,34) I,E(1),E(2),E(3),EZ,EX,THETAD,SIGZ,SIGX,TS(I,J),
     1SS(I,J)
   34 FORMAT (/1X,I2,1X,5E13.5,F8.2,4E13.5)
   31 CONTINUE
   30 CONTINUE
      IF (NPTS.EQ.1) GO TO 1000
      DO 35 J=1,4
      CALL HARMON (TS(1,J),24HTENSILE STRESS  LB/SQ IN,24,J,NPTS,RM(J))
   35 CONTINUE
      DO 36 J=1,4
      CALL HARMON (SS(1,J),30HSHEARING STRESS  LB/SQ IN     ,30,J,NPTS,
     1RM(J))
   36 CONTINUE
      GO TO 1000
      END
```

```
$IBFTC SSHARM  LIST,DECK,REF
C       PART 5 SUBROUTINE HARMON
C       HARMONICALLY ANALYSES A FUNCTION GIVEN AT IA POINTS.MAX IA=90
        SUBROUTINE HARMON (FN,BCD,NBCD,NS,IA,RM)
        DIMENSION  A(44),B(44),GAM(44),AA(44),BCD(12),CPHE(90,44),
       1SPHE(90,44),FN(90)
        DATA KOUNT/0/
        IF (KOUNT.EQ.1) GO TO 70
        PI = 3.1415926536
        TPI=2.0*PI
        DPR = 180.0/PI
        FIA = FLOAT(IA)
        TDA = 2.0/FIA
        NFC = (IA-1)/2
        DO 80  I=1,IA
        FI=FLOAT(I)
        DO 90  NN=1,NFC
        FNN=FLOAT(NN)
        XC=FNN*(FI-1.0)/FIA
        XC=AMOD(XC,1.0)
        PHE=XC*TPI
        CPHE(I,NN)=COS(PHE)
        IF (ABS(CPHE(I,NN)).LE. .0001) CPHE(I,NN)=0.0
        SPHE(I,NN)=SIN(PHE)
        IF (ABS(SPHE(I,NN)).LE. .0001) SPHE(I,NN)=0.0
   90 CONTINUE
   80 CONTINUE
        KOUNT = 1
   70 DO 10  NN=1,NFC
        A(NN) = 0.0
        B(NN) = 0.0
        DO 20  I=1,IA
        A(NN) = A(NN)+FN(I)*CPHE(I,NN)
        B(NN) = B(NN)+FN(I)*SPHE(I,NN)
   20 CONTINUE
        A(NN) = TDA*A(NN)
        B(NN) = TDA*B(NN)
        ARGAA = A(NN)**2+B(NN)**2
        AA(NN) = SQRT(ARGAA)
        IF (A(NN).NE. 0.0 .OR. B(NN) .NE. 0.0) GO TO 30
        GAM(NN) = -0.0
        GO TO 10
   30 GAM(NN) = -ATAN2(B(NN),A(NN))
        GAM(NN) = GAM(NN)*DPR
   10 CONTINUE
        AZERO = 0.0
        DO 40  I=1,IA
        AZERO = AZERO+FN(I)
   40 CONTINUE
        AZERO = AZERO/FIA
        NBW=NBCD/6
        WRITE (6,41) (BCD(I),I=1,NBW)
   41 FORMAT(1H1,39X,40HFOURIER COEFFICIENTS AND PHASE ANGLES OF,
      11X,12A6)
```

```
      IF (NS.NE.0) WRITE (6,42) NS,RM
   42 FORMAT (18H BLADE SEGMENT NO.,I3/8H RADIUS=,G12.5,4H FT.)
      WRITE (6,51) AZERO
   51 FORMAT (//45X,8HA(ZERO)=G11.4/)
      WRITE (6,50)
   50 FORMAT    (13X,14HHARMONIC ORDER,10X,4HA(N),16X,4HB(N),15X,5HAA(N),
     114X,6HGAM(N)/)
      DO 60  NN=1,NFC
      WRITE (6,52) NN,A(NN),B(NN),AA(NN),GAM(NN)
   60 CONTINUE
   52 FORMAT (18X,I2,4X,4(10X,G11.4)/)
      RETURN
      END
```

Unclassified

Security Classification

DOCUMENT CONTROL DATA - R&D

(Security classification of title, body of abstract and indexing annotation must be entered when the overall report is classified)

1. ORIGINATING ACTIVITY *(Corporate author)*
Cornell Aeronautical Laboratory, Inc.
Buffalo, New York

2a. REPORT SECURITY CLASSIFICATION
Unclassified

2b GROUP

3 REPORT TITLE

Performance and Stresses Obtained on an Isolated VTOL-Type Propeller Operating in Hovering, Transitional, and Axial Flight

4. DESCRIPTIVE NOTES *(Type of report and inclusive dates)*

5. AUTHOR(S) *(Last name, first name, initial)*

Trenka, Andrew R.

6. REPORT DATE	7a. TOTAL NO. OF PAGES	7b. NO. OF REFS
August 1967	94	5

8a. CONTRACT OR GRANT NO.	9a. ORIGINATOR'S REPORT NUMBER(S)
DA 44-177-AMC-75(T)	USAAVLABS Technical Report 67-37
b. PROJECT NO. Task 1F125901A142	
c.	9b. OTHER REPORT NO(S) *(Any other numbers that may be assigned this report)*
d.	BB-1846-S-2

10. AVAILABILITY/LIMITATION NOTICES

Distribution of this document is unlimited.

11. SUPPLEMENTARY NOTES	12. SPONSORING MILITARY ACTIVITY
	U. S. Army Aviation Materiel Laboratories, Fort Eustis, Virginia

13 ABSTRACT

Experimental performance and blade stresses measured on a three-bladed VTOL-type propeller tested in free air are presented. The isolated propeller was tested over ranges of prop speed, forward velocity, blade angle setting, and thrust axis to free-stream angle.

Correlation with a theoretical method of predicting propeller performance and blade stresses was made. It was found that when the propeller was operating in a flight condition for which the theory was developed, correlation between theory and experiment was good. When the propeller was operating in a flight condition where very small positive or negative effective angles of attack were encountered, correlation between theory and experiment was poor.

DD FORM 1 JAN 64 1473

Unclassified

Security Classification

Unclassified

Security Classification

14. KEY WORDS	LINK A		LINK B		LINK C	
	ROLE	WT	ROLE	WT	ROLE	WT
Propeller Performance Stresses Experimental Propeller Performance Experimental Stresses						

INSTRUCTIONS

1. **ORIGINATING ACTIVITY:** Enter the name and address of the contractor, subcontractor, grantee, Department of Defense activity or other organization *(corporate author)* issuing the report.

2a. **REPORT SECURITY CLASSIFICATION:** Enter the overall security classification of the report. Indicate whether "Restricted Data" is included. Marking is to be in accordance with appropriate security regulations.

2b. **GROUP:** Automatic downgrading is specified in DoD Directive 5200.10 and Armed Forces Industrial Manual. Enter the group number. Also, when applicable, show that optional markings have been used for Group 3 and Group 4 as authorized.

3. **REPORT TITLE:** Enter the complete report title in all capital letters. Titles in all cases should be unclassified. If a meaningful title cannot be selected without classification, show title classification in all capitals in parenthesis immediately following the title.

4. **DESCRIPTIVE NOTES:** If appropriate, enter the type of report, e.g., interim, progress, summary, annual, or final. Give the inclusive dates when a specific reporting period is covered.

5. **AUTHOR(S):** Enter the name(s) of author(s) as shown on or in the report. Enter last name, first name, middle initial. If military, show rank and branch of service. The name of the principal author is an absolute minimum requirement.

6. **REPORT DATE:** Enter the date of the report as day, month, year; or month, year. If more than one date appears on the report, use date of publication.

7a. **TOTAL NUMBER OF PAGES:** The total page count should follow normal pagination procedures, i.e., enter the number of pages containing information.

7b. **NUMBER OF REFERENCES:** Enter the total number of references cited in the report.

8a. **CONTRACT OR GRANT NUMBER:** If appropriate, enter the applicable number of the contract or grant under which the report was written.

8b, 8c, & 8d. **PROJECT NUMBER:** Enter the appropriate military department identification, such as project number, subproject number, system numbers, task number, etc.

9a. **ORIGINATOR'S REPORT NUMBER(S):** Enter the official report number by which the document will be identified and controlled by the originating activity. This number must be unique to this report.

9b. **OTHER REPORT NUMBER(S):** If the report has been assigned any other report numbers *(either by the originator or by the sponsor)*, also enter this number(s).

10. **AVAILABILITY/LIMITATION NOTICES:** Enter any limitations on further dissemination of the report, other than those imposed by security classification, using standard statements such as:

(1) "Qualified requesters may obtain copies of this report from DDC."

(2) "Foreign announcement and dissemination of this report by DDC is not authorized."

(3) "U. S. Government agencies may obtain copies of this report directly from DDC. Other qualified DDC users shall request through _____."

(4) "U. S. military agencies may obtain copies of this report directly from DDC. Other qualified users shall request through _____."

(5) "All distribution of this report is controlled. Qualified DDC users shall request through _____."

If the report has been furnished to the Office of Technical Services, Department of Commerce, for sale to the public, indicate this fact and enter the price, if known.

11. **SUPPLEMENTARY NOTES:** Use for additional explanatory notes.

12. **SPONSORING MILITARY ACTIVITY:** Enter the name of the departmental project office or laboratory sponsoring *(paying for)* the research and development. Include address.

13. **ABSTRACT:** Enter an abstract giving a brief and factual summary of the document indicative of the report, even though it may also appear elsewhere in the body of the technical report. If additional space is required, a continuation sheet shall be attached.

It is highly desirable that the abstract of classified reports be unclassified. Each paragraph of the abstract shall end with an indication of the military security classification of the information in the paragraph, represented as *(TS), (S), (C), or (U)*.

There is no limitation on the length of the abstract. However, the suggested length is from 150 to 225 words.

14. **KEY WORDS:** Key words are technically meaningful terms or short phrases that characterize a report and may be used as index entries for cataloging the report. Key words must be selected so that no security classification is required. Identifiers, such as equipment model designation, trade name, military project code name, geographic location, may be used as key words but will be followed by an indication of technical context. The assignment of links, rules, and weights is optional.

Unclassified

Security Classification